

Improving Chest X-Ray Report Generation by Leveraging Warm-Starting

Aaron Nicolson[†], Jason Dowling[†], and Bevan Koopman[†]

[†]Australian e-Health Research Centre, Commonwealth Scientific and Industrial Research Organisation, Herston 4006, Queensland, Australia

Abstract—Automatically generating a report from a patient’s Chest X-Rays (CXRs) is a promising solution to reducing clinical workload and improving patient care. However, current CXR report generators—which are predominantly encoder-to-decoder models—lack the diagnostic accuracy to be deployed in a clinical setting. To improve CXR report generation, we investigate warm-starting the encoder and decoder with recent open-source computer vision and natural language processing checkpoints, such as the Vision Transformer (ViT) and PubMedBERT. To this end, each checkpoint is evaluated on the MIMIC-CXR and IU X-Ray datasets using natural language generation and Clinical Efficacy (CE) metrics. Our experimental investigation demonstrates that the Convolutional vision Transformer (CvT) ImageNet-21K and the Distilled Generative Pre-trained Transformer 2 (DistilGPT2) checkpoints are best for warm-starting the encoder and decoder, respectively. Compared to the state-of-the-art (\mathcal{M}^2 Transformer Progressive), CvT2DistilGPT2 attained an improvement of 8.3% for CE F-1, 1.8% for BLEU-4, 1.6% for ROUGE-L, and 1.0% for METEOR. The reports generated by CvT2DistilGPT2 are more diagnostically accurate and have a higher similarity to radiologist reports than previous approaches. By leveraging warm-starting, CvT2DistilGPT2 brings automatic CXR report generation one step closer to the clinical setting. CvT2DistilGPT2 and its MIMIC-CXR checkpoint are available at <https://github.com/aehrc/cvt2distilgpt2>.

Index Terms—CvT2DistilGPT2, Medical image analysis, Chest X-Ray, Report Generation

I. INTRODUCTION

The chest radiograph or Chest X-Ray (CXR) is an indispensable tool for diagnosing diseases of the cardiovascular and respiratory systems [1]. While it is the most commonly performed radiologic examination, the CXR is difficult to interpret [2]. Even though CXRs are analysed by clinicians of all types, radiologists demonstrate the highest diagnostic accuracy [3]. Alarmingly, the workload of radiologists has increased significantly over the last couple of decades—mostly due to increases in cross-sectional imaging and understaffing [4], [5]. As a consequence, burnout is common amongst radiologists, with fatigue leading to a reduction in their diagnostic accuracy [6], [7]. Radiologists also exhibit interobserver and intraobserver variability in their diagnoses [8]. Currently, radiologists communicate their findings to referring clinicians through a report. However, there is inconsistency in reporting styles, with structured reports recommended [9]. Moreover, failing to report in a clear and concise manner—which is

exacerbated by fatigue—can also lead to sub-optimal patient care [10], [11]. From this, it is clear that CXR interpretation could be improved by reducing the workload of radiologists.

An emerging solution is the use of machine learning to automatically generate a report from one or more CXRs [12]. An automatic CXR report generation system could improve the efficiency of interpretation and report creation by providing a reference report to radiologists. Such a system could also increase the diagnostic accuracy of clinicians who have a lower diagnostic confidence [13], [14]. A hosted system would also be able to serve the radiology demands of an entire health system, as it possesses the ability to remotely interpret multiple CXRs simultaneously in seconds. Moreover, the system would not suffer from intraobserver variability or fatigue—which could result in more consistent reporting [15]. While current CXR report generation approaches are promising, a significant improvement in diagnostic accuracy is needed before adoption into a clinical setting [16].

The most popular approach to automatic CXR report generation is with a deep learning encoder-to-decoder model [12]. The encoder produces visual features from a CXR and is typically a Convolutional Neural Network (CNN), such as a Residual or Densely-connected Network (ResNet or DenseNet, respectively) [17], [18]. A CNN includes multiple layers of two-dimensional convolutional kernels that have an inductive bias towards local spatial features—a characteristic that makes CNNs suitable for Computer Vision (CV) tasks. The visual features are then observed by the decoder, which autoregressively generates a report. Current approaches employ a Transformer as the decoder [19]. A Transformer consists of layers that have multiple attention heads, where attention produces an output based on which inputs it deems important. For Natural Language Processing (NLP), each input corresponds to a word (or subword). Along with the encoder-to-decoder model, several deep learning techniques have been shown to improve CXR report generation.

One such technique is warm-starting the encoder before training the encoder-to-decoder model on the CXR report generation task. Warm-starting refers to the initialisation of a model’s parameters with those of a pre-trained checkpoint. A checkpoint includes the values of all the learned parameters of a trained model. The transfer of knowledge from the pre-training task to the final task can provide a significant performance boost, particularly when the pre-training dataset

Corresponding author: A. Nicolson (email: aaron.nicolson@csiro.au).

is significantly larger than that of the final task. Furthermore, warm-starting is particularly effective when the domain of the pre-training task is similar to that of the final task. For CXR interpretation, warm-starting the encoder with a general-domain CV checkpoint—typically a ResNet or DenseNet ImageNet-1K checkpoint—provides a significant performance boost over random parameter initialisation [20], [21], [12]. More recently, DistilGPT2—a general-domain NLP checkpoint—was used to warm-start the decoder [22]. However, a direct comparison to a randomly initialised decoder was not provided. While warm-starting the encoder has become standard practice, and warm-starting the decoder is beginning to receive traction, there exists a plethora of general-domain and domain-specific CV and NLP checkpoints that have yet to be explored for CXR report generation.

General-domain CV checkpoints have received a considerable amount of attention as of late [23]. Various pre-training tasks, such as distillation and self-supervised learning, have produced checkpoints that provide a significant performance boost on general-domain tasks [24], [25]. Along with these, several prominent CV models and their checkpoints have not been investigated for CXR report generation. ImageNet-1K checkpoints for EfficientNet are one such example; EfficientNet is a CNN that can outperform ResNets and DenseNets while consuming drastically fewer parameters [26]. Another promising checkpoint is the Vision Transformer (ViT) and its improvements [27], [28], [29]. ViT is a Transformer that has been trained on large general-domain image classification datasets, where the set of words as input are replaced with a set of patches from an image. Transformers possess several benefits over CNNs, such as no pooling, a full-receptive field at each layer, and robustness to occlusion [30]. More recent checkpoints that use distillation have outperformed EfficientNet on ImageNet-1K, namely the Data-efficient image Transformer (DeiT) [25].

While DistilGPT2 has been investigated for CXR report generation, several other prominent NLP checkpoints have not. General-domain NLP checkpoints formed from large corpora, such as BERT and GPT2, have been shown to boost performance in Natural Language Understanding (NLU) [31] and Natural Language Generation (NLG) [32] tasks, respectively. NLU focuses on comprehending natural language through grammar and context while NLG focuses on constructing natural language based on a given input. As BERT is an NLU checkpoint, one would assume that it is less suitable than GPT2 for warm-starting a decoder. However, Rothe *et al.* disproved this by demonstrating that BERT is more apt than GPT2 for warm-starting the decoder of a sequence-to-sequence model [33, BERT2BERT vs. BERT]. Following BERT, several NLU checkpoints were developed from large biomedical natural language corpora. Warm-starting with a biomedical NLU checkpoint instead of BERT was shown to improve performance in biomedical NLU tasks [34]. As highlighted by Kaur *et al.*, warm-starting the decoder of a CXR report generator with a biomedical NLU checkpoint is a promising approach that warrants investigation [35]. Hence, an investiga-

tion determining if NLP checkpoints can be effectively fine-tuned to model not only CXR reports but also visual features of CXRs is called for.

In this work, we study the impact of warm-starting on CXR report generation. We do this by evaluating various general-domain and domain-specific pre-trained checkpoints on the MIMIC-CXR and IU X-Ray datasets (described in Section III) using NLG and Clinical Efficacy (CE) metrics (described in Section V-B). From this evaluation, we determine which pre-trained checkpoints are most suitable for warm-starting the encoder and decoder of a CXR report generator. Using these checkpoints, we aim to outperform previous approaches in the literature. We also aim to answer the following Research Questions (RQs):

- RQ1:** If Transformer-based CV checkpoints are better than CNN-based checkpoints for warm-starting the encoder.
- RQ2:** If an NLP checkpoint can be effectively fine-tuned to model not only natural language but also visual features.
- RQ3:** If BERT is a better pre-trained checkpoint than GPT2 for warm-starting the decoder.
- RQ4:** If domain-specific checkpoints are better than general-domain checkpoints for warm-starting the encoder and decoder.

We also aim to instil the knowledge that the best checkpoint for a task can be influenced by many variables, such as the domain and size of the training data, the model architecture, the pre-training task, and the vocabulary. This investigation also enables us to give insightful recommendations on how to further improve CXR report generation.

II. RELATED WORK

A. CXR report generation

In this section, we summarise both foundational and recent automatic CXR report generation approaches in the literature. For a more exhaustive review of CXR report generation, we refer the reader to the survey conducted by Kaur *et al.* [35]. As highlighted by Pavlopoulos *et al.*, the MIMIC-CXR and IU X-Ray datasets are consistently used in the literature to evaluate CXR report generation (both are described in Subsection III) [12]. The following approaches are evaluated using at least one or both of these datasets.

Wang *et al.* was the first to use an end-to-end encoder-to-decoder model for CXR report generation—a ResNet-502RNN with attention, where RNN refers to a Recurrent Neural Network.¹ The authors employed multi-task learning of CXR report generation (IU X-Ray) and multi-label abnormality classification (ChestX-ray14 abnormality labels [36]). The ResNet was warm-started using an ImageNet-1K checkpoint. The proposed approach outperformed a general-domain image

¹Henceforth, the naming convention for encoder-to-decoder models will be the name of the encoder, followed by 2, followed by the name of the decoder. For example, a model with a CNN encoder and an RNN decoder will be named CNN2RNN.

captioning approach, where several NLG metrics were used for evaluation. However, many false negative abnormality predictions were evident in the generated reports [36, Figure 4].

While NLG metrics capture the similarity between the predicted and ground truth reports, they do not always capture diagnostic accuracy [12]. Motivated by this, Liu *et al.* proposed the Clinical Efficacy (CE) metric [37]. The CE metric makes use of the CheXpert labeler—a tool developed for extracting 14 observations from the reports of the CheXpert dataset (12 of which are abnormalities) [38]. For each observation, the CheXpert labeler predicts whether each observation was mentioned as positive, negative, or uncertain; or if it was not mentioned. For the CE metric, observations are first extracted from the generated and ground truth reports using the CheXpert labeler. Following this, the precision, recall, and F-1 score between the observations of the generated and ground truth reports are calculated to give the scores of the CE metric. Liu *et al.* used the CE metric as the reward for Self-Critical Sequence Training (SCST), in place of an NLG metric. SCST enables the decoder to be fine-tuned with its own outputs as input—something that is not possible with standard training schema [39]. This is achieved by using a reinforcement learning algorithm that uses the score between the generated and ground truth reports as the reward. This was able to outperform the approach by Wang *et al.* for all tested NLG metrics [36]. Moreover, using the CE metric scores as the reward for SCST was shown to improve the diagnostic accuracy of the generated reports.

To embed expert knowledge, Zhang *et al.* incorporated a Graph Convolutional Network (GCN)—whose nodes consisted of abnormalities—into the encoder [40]. This was able to outperform the aforementioned CXR report generation approaches on multiple NLG metrics. The authors also developed a diagnostic accuracy metric based on the graph CNN—which showed that the graph CNN improves diagnostic accuracy.

More recently, Lovelace and Mortazavi employed a CNN followed by a series of Transformer layers as the encoder and a Transformer decoder. To improve diagnostic accuracy, the CheXpert labeler was used to extract observations from the generated report in a differentiable manner, where the loss between the observations of the generated and ground truth reports was added to the training loss. This outperformed multiple approaches that employed an RNN as the decoder, where multiple NLG metrics and the CE metric were used for evaluation [41].

Chen *et al.* proposed a “memory-driven” Transformer decoder (R2Gen) [42], which later included “Cross-modal Memory” (CMN) [43]. Using multiple NLG metrics and the CE metric, it was determined that the proposed approaches were able to outperform several previous CXR report generation approaches in the literature, each of which used an RNN as the decoder [44], [45], [46].

Alfarghaly *et al.* employed CheXNet—a DenseNet-121 ChestX-ray14 checkpoint—as the encoder and a Transformer as the decoder. The decoder was warm-started with Distil-

GPT2, a general-domain NLG checkpoint. However, cross-attention was not used with each layer of the decoder, rather the embeddings of each predicted abnormality of CheXNet were fed as input to DistilGPT2. This method outperformed multiple approaches that utilised an RNN as the decoder for multiple NLG metrics [22].

Liu *et al.* proposed the Contrastive Attention model which compares the visual features of the current CXR to a pool of CXRs that have no abnormalities, where a ResNet-50 warm-started with a CheXpert checkpoint was used to extract the visual features. Contrastive Attention comprises two modules, ‘aggregate attention’ and ‘difference attention’. Aggregate attention finds the normal CXRs from the pool that are closest to the CXR in question. Difference attention involves two steps; for the first step, common features between the current CXR and the pool of normal CXRs are found. For the second step, the common features are subtracted from the features of the current CXR to capture ‘contrastive information’. This was able to outperform R2Gen, where multiple NLG metrics and the CE metric were used for evaluation [47].

With the aim to imitate the interpretation process of radiologists, Liu *et al.* proposed the *a Posterior-and-Prior* Knowledge Exploring-and-Distilling approach (PPKED) [48]. Along with a CXR, the model consumes embeddings of the most common abnormalities found in the reports from the training set. It also consumes encoded reports from CXRs of the training set that have similar visual features to the current CXR. Finally, the model consumes the embedding from a knowledge graph that represents the most common abnormalities found in the training set. This outperformed R2Gen, where multiple NLG metrics and the CE metric were used for evaluation [47].

Nooralahzadeh *et al.* proposed an approach that generated a report from detected abnormalities in the CXR [49]. First, a DenseNet-121 extracted visual features from a CXR, where a pre-trained CheXpert checkpoint was used for warm-starting. Next, an encoder-to-decoder model called the meshed Transformer with memory (\mathcal{M}^2 Transformer) [50] predicted the abnormalities from the visual features. The labels for the \mathcal{M}^2 Transformer were extracted from the CXR using the GCN of Zhang *et al.* [40]. These were fed to BART to generate the report, where BART is a sequence-to-sequence encoder-to-decoder model [51]. The final method, named \mathcal{M}^2 Transformer Progressive, outperformed R2Gen, where multiple NLG metrics and the CE metric were used for evaluation [47].

B. CV checkpoints

As highlighted in the previous subsection, the encoder is typically warm-started with a ResNet or DenseNet ImageNet-1K or CXR checkpoint. These are summarised in this section, along with more recent CV models and their associated checkpoints.

Residual and dense aggregations of layer outputs have been found to benefit training. Residual aggregations simplify the landscape of the loss function and prevent the vanishing and exploding gradient problems [17]. This allows the training of

very deep CNNs, called ResNets. The dense aggregations of DenseNet offer direct feature re-usage, as deeper layers have access to the outputs of shallower layers [18]. Following this, Tan *et al.* focused on efficiently scaling the depth, width, and input image size of CNNs, forming EfficientNets. As a result, EfficientNets are able to significantly outperform ResNets and DenseNets on ImageNet-1K, while remaining parameter efficient [26]. An EfficientNet as the encoder, warm-started or not, has not been investigated for CXR report generation. Domain-specific CXR checkpoints for CNNs also exist in the literature. Rajpurkar *et al.* proposed CheXNet, a DenseNet-121 checkpoint for multi-label classification of 14 abnormalities. The checkpoint was formed by additionally training an ImageNet-1K checkpoint on ChestX-Ray14 [52].

More recently, Transformers have been investigated for CV. Dosovitskiy *et al.* proposed the Vision Transformer (ViT)—a Transformer checkpoint pre-trained on large general-domain image classification datasets which takes as input a set of patches from an image [27]. ViT possesses several appealing features for CV, including no pooling, a full-receptive field, and robustness to occlusion [30]. However, ViT does not possess the same inductive bias that makes CNNs an attractive option for medical CV tasks—a bias towards local spatial features. While the self-attention weights of a ViT head are able to model the relationship between patches, they do not model the relationship between pixels. This may be detrimental for CXR report generation, as many anatomical features of the chest—such as the pulmonary arteries—are represented in fine detail by the CXR. Moreover, ViT was only able to outperform ResNet when warm-starting with checkpoints that have been trained using 30 million or more images [27, Figure 4, ViT-B/32 vs. ResNet50x1 (BiT)]. This lead to Dosovitskiy *et al.* concluding that ViT does not generalise well when trained on insufficient amounts of data.

There are multiple improvements to ViT in the literature that either use a self-supervised pre-training task or modify the Transformer to manually inject an inductive bias towards local spatial features. The Convolutional vision Transformer (CvT) replaces the linear layers of each self-attention head with two-dimensional convolutional layers, thus introducing an inductive bias to local spatial features into each head. This enabled CvT to outperform ViT on ImageNet-1K [28]. The Data-efficient image Transformer (DeiT) is an ImageNet-1K checkpoint that incorporated knowledge distillation into its set of pre-training tasks. Knowledge distillation involves two models; a smaller model—called the student—and a larger model—called the teacher. The student is trained to replicate the categorical distribution of the teacher. For DeiT, the teacher was a recent CNN. On ImageNet-1K, DeiT was able to outperform ViT and EfficientNet [25].

The Cross-Covariance image Transformer (XCiT) utilises a transposed version of the self-attention mechanism. This results in the attention weights modelling the relationship between feature channels rather than patches. To model the relationship between local patches, each layer of XCiT employs a two-dimensional convolutional kernel. XCiT was able

to outperform both EfficientNet and DeiT on ImageNet-1K [29]. Inspired by BERT, Bao *et al.* used a self-supervised task, namely Masked Image Modelling (MIM), to form a Bidirectional Encoder representation from an image Transformer (BEiT). For MIM, the objective for each randomly masked patch is to predict its corresponding discrete visual token. The token for each patch was produced by a discrete Variational Auto-Encoder (VAE). BEiT was able to outperform both ViT and DeiT on ImageNet-1K [24].

C. NLP checkpoints

As detailed in Subsection II-A, the Transformer is the standard decoder used by recent CXR report generation methods. In this subsection, we summarise the Transformer and its checkpoints. Vaswani *et al.* proposed the Transformer—a sequence-to-sequence model for NLG. Its layers employ multiple scaled dot-product attention heads, each of which models the complex dependencies between its inputs. Due to this, Transformers more efficiently model long-range dependencies between subword tokens than RNNs and Temporal Convolutional Networks (TCNs) [19, Table 1].

Building upon this, checkpoints for the encoder and decoder of the Transformer were formed with self-supervised pre-training tasks and extremely large, unlabelled corpora. Masked Language Modelling (MLM) and Next Sentence Prediction (NSP) are self-supervised pre-training tasks that were used to form Bidirectional Encoder Representations from Transformers (BERT)—a general-domain NLU checkpoint created from BookCorpus [53] and English Wikipedia. As the encoder is non-causal, an output for BERT depends on all input tokens during MLM and NSP, and not just previous tokens. This enabled BERT to outperform previous Transformer checkpoints on multiple NLU tasks [31]. The second version of the Generative Pre-trained Transformer (GPT2) is a checkpoint for the decoder of the Transformer. Using language modelling as the pre-training task and the WebText corpus [32], GPT2 achieved state-of-the-art performance on several zero-shot NLG tasks [32].

Sanh *et al.* proposed DistilBERT, a distilled version of BERT that consumes 40% fewer parameters while retaining 97% of its performance. Knowledge distillation was incorporated into the training task, where DistilBERT was the student and BERT was the teacher. The authors also produced DistilGPT2 in a similar fashion [54].

The self-supervised tasks used to form BERT (namely MLM and NSP) have been used to form domain-specific NLU checkpoints. Beltagy *et al.* formed a scientific NLU checkpoint from 1.14M documents of Semantic Scholar—a corpus of scientific publications. The resulting checkpoint, called SciBERT, outperformed BERT on several scientific NLU tasks. SciBERT also featured a domain-specific vocabulary constructed from Semantic Scholar [55]. Multiple domain-specific checkpoints have been formed from biomedical corpora, particularly PubMed and PubMed Central (PMC). As seen in Table I, a benefit of PubMed and PMC is that they are both larger in size than the corpora used to train BERT

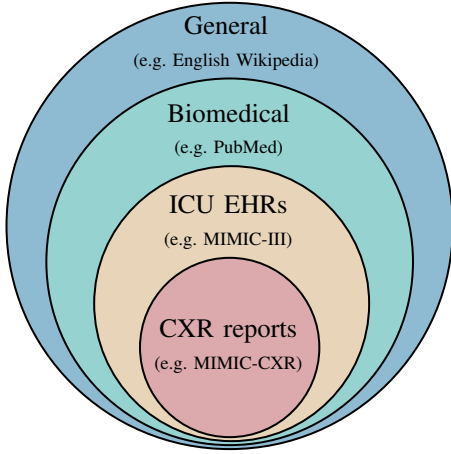


Fig. 1. Non-proportional Venn diagram of the vocabulary of each natural language domain. As CXR reports are included in Intensive Care Unit (ICU) Electronic Health Records (EHRs), the vocabulary of CXR reports is a subset of the vocabulary of ICU EHRs. The vocabulary of ICU EHRs is a subset of the vocabulary of biomedical natural language, which is a subset of the vocabulary of the general domain. An example of a corpus belonging to each domain is also given.

TABLE I
SIZES OF THE DATASETS USED TO CREATE THE CHECKPOINTS. THE NUMBER OF EXAMPLES FOR SEMANTIC SCHOLAR ARE THOSE USED TO PRE-TRAIN SCIBERT [55].

Dataset	No. of examples
ImageNet-21K [56]	14M images
ImageNet-1K [21]	1.3M images
CheXpert [38]	224K images
BookCorpus [53]	0.8B words
English Wikipedia	2.5B words
WebText [32]	8M documents
Semantic Scholar [57]	1.14M papers [55]
PubMed	4.5B words
PMC	13.5B words
MIMIC-III [58]	2M notes

and GPT2 (BookCorpus, English Wikipedia, and WebText). BioBERT is one such example, which outperformed BERT on several biomedical NLU tasks. However, BioBERT does not have a domain-specific vocabulary, instead it is inherited from BERT. This may be less than optimal, as medical terms not captured by BERT’s vocabulary would be represented by multiple subwords [34]. PubMedBERT improves upon BioBERT by having a domain-specific vocabulary built from PubMed and PMC. The authors also demonstrate that training from scratch rather than additionally training a general-domain checkpoint such as BERT is best for biomedical NLU tasks—if there is sufficient data [59].

There also exists multiple checkpoints formed from MIMIC-III—an Intensive Care Unit (ICU) Electronic Health Record (EHR) corpus. As seen in Figure 1, the vocabulary of EHRs is a subset of the vocabulary of biomedical natural language. ClinicalBERT is an EHR NLU checkpoint formed by further training BioBERT with MLM and NSP on MIMIC-III [60]. A similar checkpoint is BlueBERT, which is formed in two stages: BERT is further trained with MLM and NSP

on PubMed. The resulting checkpoint is further trained with MLM and NSP on MIMIC-III, finally forming BlueBERT [61]. Both ClinicalBERT and BlueBERT were able to outperform BioBERT on several EHR NLU tasks. However, ClinicalBERT and BlueBERT do not have domain-specific vocabularies and instead rely on the vocabulary of BERT. Moreover, MIMIC-III is considerably smaller in size than the other corpora listed in Table I, raising concerns as to whether ClinicalBERT and BlueBERT can be successfully fine-tuned to CXR report generation.

D. Our contributions

Our study differs from previous studies as follows:

- Unlike previous studies that only consider a single checkpoint for the encoder and/or decoder, we investigate the impact of the checkpoint choice on CXR report generation.
- We investigate CV models and their checkpoints that have not been considered for CXR report generation, namely, EfficientNet and Transformer-based CV models.
- We investigate NLP checkpoints, specifically, NLU checkpoints such as BERT, and NLG checkpoints such as GPT2.
- We investigate domain-specific CV and NLP checkpoints.
- We present a case study of the final model that includes the attention weights of its cross-attention heads—to reveal what the model attends to when generating a report.

Moreover, we perform a more fine-grained evaluation on individual abnormalities; where earlier studies performed such fine-grained evaluations (e.g., Liu *et al.* [37]), later studies only provided averaged results over individual abnormalities.

III. DATASETS

The Medical Information Mart for Intensive Care CXR dataset (**MIMIC-CXR**) consists of 377,110 CXRs in both DICOM and JPEG formats, and 227,835 English radiology reports associated with 64,588 patients. The reports and CXRs were automatically de-identified [62], [63]. Demner-Fushman *et al.* released a dataset called **IU X-Ray** that consisted of 3,955 English radiology reports and 7,470 CXRs in both DICOM and PNG formats, where both the reports and CXRs were de-identified automatically. Each report is associated with a single patient [64]. We refer the reader to the survey conducted by Pavlopoulos *et al.* for a more detailed analysis of MIMIC-CXR and IU X-Ray [12, Subsection 2.1].

In order to compare to previous studies, we adopt the dataset splits of Chen *et al.* for both MIMIC-CXR and IU X-Ray [42].² Chen *et al.* used the *findings* section of each ground truth report as the label and excluded examples that had reports without a findings section. For MIMIC-CXR, the subsets are formed from 276,778 of the CXRs. A portion of the reports were associated with multiple CXRs, meaning

²The MIMIC-CXR and IU X-Ray subsets used by Chen *et al.* are available at: <https://github.com/cuhksz-nlp/R2Gen>.

TABLE II
SUBSET SPLITS OF MIMIC-CXR AND IU X-RAY FROM CHEN *et al.* [42].

Dataset	No. of examples			Pixel depth	Views per example
	Training	Validation	Test		
MIMIC-CXR (Chen <i>et al.</i> splits [42])	270,790	2,130	3,858	8-bit	1
IU X-Ray (Chen <i>et al.</i> splits [42])	2,069	296	590	8-bit	2

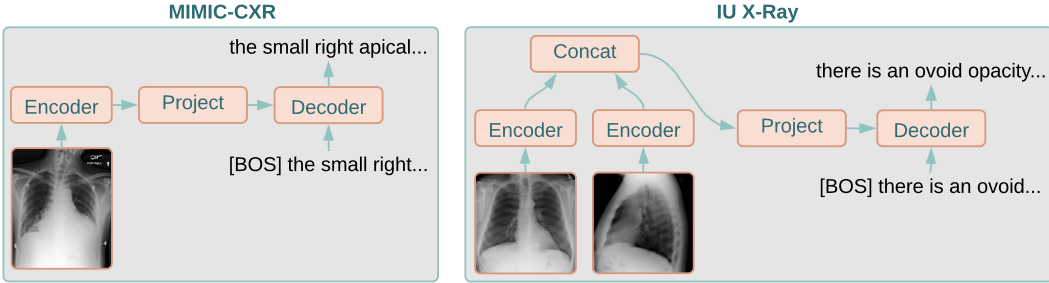


Fig. 2. CXR report generation framework for (left) MIMIC-CXR and (right) IU X-Ray as in Chen *et al.* [42]. [BOS] is the beginning-of-sentence special token.

that they were the label for multiple examples. The subset splits are detailed in Table II; the 276,778 CXRs are split into 270,790, 2,130, and 3,858 reports for training, validation, and testing, respectively. For IU X-Ray, the subsets are formed from 2,955 of the reports, where each report is associated with a frontal and lateral view. This means that the model consumes two CXRs per example for IU X-Ray. The 2,955 reports are split into 2,069, 296, and 590 reports for training, validation, and testing, respectively. A training example for IU X-Ray is shown in Figure 2 (right); the frontal and lateral views are given as input to the encoder and the label is the ground truth report produced by a radiologist. For both MIMIC-CXR and IU X-Ray, each patient is included in only one of the subsets.

IV. PROBLEM FORMULATION

Given a set of N CXRs $\mathcal{X} = \{\mathbf{X}_0, \dots, \mathbf{X}_{N-1}\}$ where $\mathbf{X}_i \in \mathbb{R}^{C \times W \times H}$ and C , W , and H denote the number of channels, the width, and the height of each CXR, respectively, the aim is to generate a report (\hat{R}) whose target is the findings section of the ground truth report R . The encoder-to-decoder model generates \hat{R} in multiple stages; first, the encoder E produces a set of visual features from each of the CXRs $\mathcal{V} = \{\mathbf{V}_0, \dots, \mathbf{V}_{N-1}\}$, where the encoder processes each CXR independently ($E : \mathbf{X}_i \rightarrow \mathbf{V}_i$), $\mathbf{V}_i \in \mathbb{R}^{S \times F}$, S is the number of spatial positions, and F is the number of features for each spatial position. Here, the visual features correspond to the last hidden state of the encoder. For some of the CV models, particularly the CNNs, the spatial positions are distributed over two axes—which are flattened to give S . Moreover, for some CV models, the spatial position and feature axes of the last hidden state are opposite (i.e. $\mathbf{V}_i \in \mathbb{R}^{F \times S}$) and must be transposed. Next, the visual features for each CXR are concatenated along the spatial position axis: $\mathbf{V}_{concat} = concat(\mathbf{V}_0, \dots, \mathbf{V}_{N-1}) \in \mathbb{R}^{D \times F}$, where

concat is the concatenation operation and $D = S \times N$. Next, the visual features are projected to the hidden size of the decoder H using learned projection matrix $\mathbf{P} \in \mathbb{R}^{F \times H}$: $\mathbf{V}_{project} = \mathbf{V}_{concat} \cdot \mathbf{P} \in \mathbb{R}^{D \times H}$.

The projected visual features are fed to the decoder via a randomly initialised multi-head cross-attention module, which is inserted between the masked multi-head self-attention module and the feedforward neural network module of each decoder layer [19, Section 3.1, Decoder]. The decoder then generates the report from the projected visual features in an autoregressive fashion ($D : \mathbf{V}_{project} \rightarrow \hat{R}$). As shown in Figure 2, $N = 1$ for MIMIC-CXR and $N = 2$ for IU X-Ray. This means that the concatenation operation is not required for MIMIC-CXR. For IU X-Ray, the two CXRs for an example correspond to a frontal and lateral view, whereas for MIMIC-CXR, the single CXR for an example is either a frontal or a lateral view, as in [42].

V. METHODOLOGY

A. Checkpoints

In this study, we investigate the CV checkpoints of Table III and the NLP checkpoints of Table IV for CXR report generation. The training data that formed each checkpoint, the vocabulary of each NLP checkpoint, and the image width of each CV checkpoint is given. Note that the image height is equal to the image width for each CV checkpoint. The configuration of each CV model is also indicated. For each decoder checkpoint, if available, we use the uncased version, else, the cased version. This was due to the lowercase format of the ground truth reports, as described in Subsection V-D. Finally, the number of parameters for each checkpoint are given in Figure 3.

TABLE III

CV CHECKPOINTS FOR WARM-STARTING THE ENCODER. CONFIGURATIONS FOR THE SAME MODEL ARE SEPARATED BY AMPERSANDS AND COMMAS. THE CONFIGURATIONS FOR RESNET, DENSENET, AND CVT INDICATE THE NUMBER OF LAYERS; THE CONFIGURATIONS FOR EFFICIENTNET INDICATE THE SIZE OF THE MODEL WITH B4 BEING THE SMALLEST AND B7 BEING THE LARGEST; THE CONFIGURATIONS FOR ViT, DeiT, AND BEiT INDICATE THE PATCH SIZE, WHERE DISTILLATION IS THE PRE-TRAINING TASK FOR DeiT; THE CONFIGURATIONS FOR XCiT ARE DETERMINED AS FOLLOWS: THE LETTER AND NUMBER COMBINATION BEFORE THE FORWARD SLASH INDICATES THE SIZE OF THE MODEL, Υ INDICATES THAT DISTILLATION WAS USED AS A PRE-TRAINING TASK, AND THE NUMBER BETWEEN THE FORWARD SLASH AND Υ INDICATES THE WIDTH AND HEIGHT OF THE PATCH SIZE.

Model	Configuration/s	Image width (W)	Pre-training data
ResNet [17]	101 & 152	224 & 224	ImageNet-1K [21]
DenseNet [18]	121, 169, & 201	224, 224, & 224	ImageNet-1K [21]
CheXNet [52]	DenseNet-121	224	ImageNet-1K [21] + CheXpert [38]
EfficientNet [26]	B4, B5, B6, & B7	380, 456, 528, & 600	ImageNet-1K [21]
ViT _{BASE} [27]	16x16	384	ImageNet-21K [56] + ImageNet-1K [21]
CvT [28]	13 & 21	384 & 384	ImageNet-21K [56]
DeiT _{BASE} [25]	16x16 w. distillation	384	ImageNet-1K [21]
XCiT [29]	S12/16 Υ , S12/8 Υ , S24/16 Υ , S24/8 Υ , & M24/16 Υ	384, 384, 384, 384, & 384	ImageNet-1K [21]
BEiT _{BASE} [24]	16x16	384	ImageNet-21K [56] + ImageNet-1K [21]

TABLE IV

NLP CHECKPOINTS FOR WARM-STARTING THE DECODER. THE SYMBOL → INDICATES THAT A CHECKPOINT WAS TRANSFERRED TO A NEW DOMAIN. THE TRANSFORMER IS IDENTICAL IN CONFIGURATION TO DISTILBERT, EXCEPT THAT ITS PARAMETERS ARE RANDOMLY INITIALISED RATHER THAN WARM-STARTED. PUBMED AND PUBMED CENTRAL (PMC) ARE AVAILABLE AT <https://pubmed.ncbi.nlm.nih.gov/> AND <https://www.ncbi.nlm.nih.gov/PMC/>, RESPECTIVELY.

Model	Cased/uncased	Pre-training data	Vocabulary
Transformer	Uncased	–	30K BookCorpus [53] + English Wikipedia
GPT2	Cased	WebText [32]	50k WebText [32]
BERT _{BASE} [31]	Uncased	BookCorpus [53] + English Wikipedia	30K BookCorpus [53] + English Wikipedia
DistilBERT _{BASE} [54]	Uncased	BookCorpus [53] + English Wikipedia	30K BookCorpus [53] + English Wikipedia
DistilGPT2 [54]	Cased	WebText [32]	50k WebText [32]
BioBERT _{BASE} [34]	Cased	BERT _{BASE} → PubMed + PMC	30K BookCorpus [53] + English Wikipedia
SciBERT _{BASE} [55]	Uncased	Semantic Scholar [57]	30K Semantic Scholar [57]
ClinicalBERT _{BASE} [60]	Cased	BioBERT _{BASE} → MIMIC-III [58]	30K BookCorpus [53] + English Wikipedia
BlueBERT _{BASE} [61]	Cased	BERT _{BASE} → PubMed → MIMIC-III [58]	30K BookCorpus [53] + English Wikipedia
PubMedBERT _{BASE} [59]	Uncased	PubMed + PMC	30K PubMed + PMC

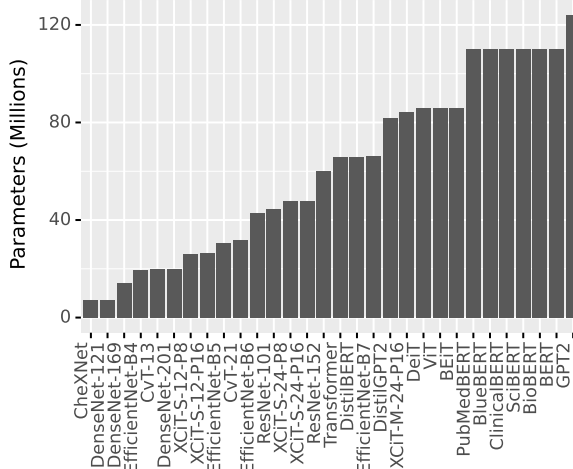


Fig. 3. The number of parameters for each checkpoint.

B. Evaluation Metrics

As in previous CXR report generation studies, we employ several NLG metrics and the Clinical Efficacy (CE) metrics to evaluate the generated reports [12]. The NLG metrics are word overlap measures that compute a similarity score based on the number of words shared between the generated and

ground truth reports. The Bi-Lingual Evaluation Understudy (**BLEU-n**) measure computes the word n -gram overlap between the generated and ground truth reports, for example, BLEU-3 considers trigrams [65]. The Metric for Evaluation of Translation with Explicit ORdering (**METEOR**) builds upon BLEU-1 by instead computing the F_β score between unigrams (where recall is weighted higher than precision). METEOR also employs stemming and synonymy matching [66].

The Recall-Oriented Understudy for Gisting Evaluation with Longest common subsequence-based statistics (**ROUGE-L**) is the harmonic mean of ROUGE-L Recall and Precision. ROUGE-L Recall is ratio of the length of the longest common n -gram shared by the generated and ground truth reports, to the number of words in the ground truth report. ROUGE-L Precision is identical to ROUGE-L Recall, except that the denominator is the number of words in the generated report [67]. The Consensus-based Image Description Evaluation (**CIDEr**) measure computes the cosine similarity between Term Frequency-Inverse Document Frequency (TF-IDF) n -grams of the generated and ground truth reports. Cosine similarities are calculated for 1 to 4-grams and their average is returned as the final score. By using TF-IDFs, terms that are infrequent in the corpus are rewarded, while terms that are common (e.g., stopwords) are penalised [68].

It should be noted that the aforementioned word overlap measures do not necessarily capture diagnostic accuracy. To

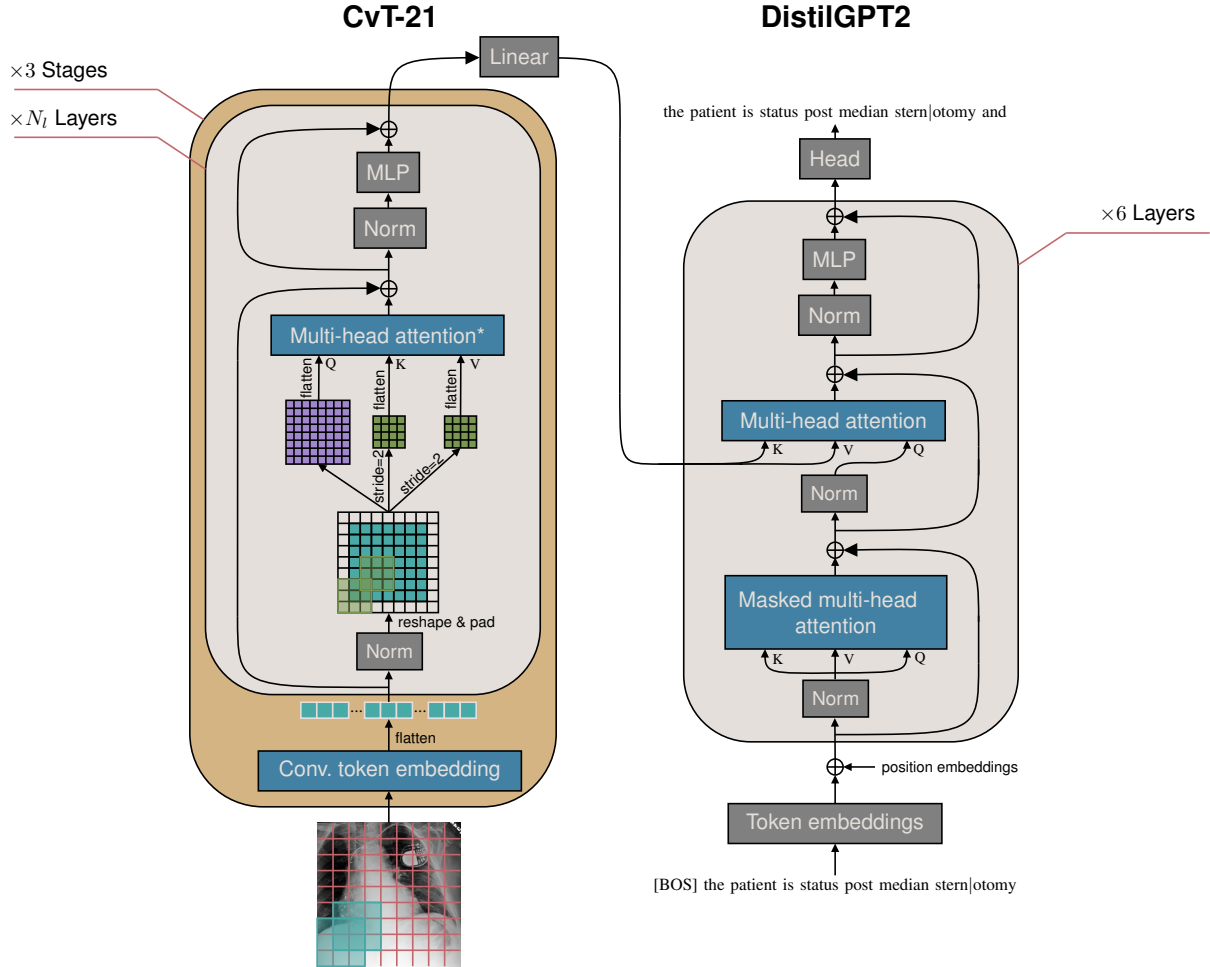


Fig. 4. CvT-21|DistilGPT2 for MIMIC-CXR with the Chen *et al.* splits [42]. Q , K , and V are the queries, keys, and values, respectively, for multi-head attention [19]. * indicates that the linear layers for Q , K , and V are replaced with the convolutional layers depicted below the multi-head attention module. [BOS] is the beginning-of-sentence special token. N_l is the number of layers for each stage, where $N_l = 1$, $N_l = 4$, and $N_l = 16$ for the first, second, and third stage, respectively. The head for DistilGPT2 is the same used for language modelling. Subwords produced by DistilGPT2 are separated by a vertical bar.

more effectively evaluate this, we use the CE metric that was previously employed to evaluate CXR report generators [37], [42]. In place of the CheXpert labeler, we use CheXbert—a BERT-based approach to extracting the 14 CheXpert observations from a given report. CheXbert demonstrated a statistically significant improvement in performance over the CheXpert labeler (CheXbert had a macro-averaged F-1 score improvement of 0.055 over the CheXpert labeler), while being 120 times faster (when a GPU is available) [69]. The CheXbert classification scores are calculated as follows; CheXbert first determines the class of each of the 14 observations from the generated and ground truth reports as either *positive*, *negative*, *uncertain*, or *no mention*.³ Next, the multi-class classification task for each observation is converted into a binary classification task; observations that are *positive* are considered

³The 14 observations include *enlarged cardiomedastinum*, *cardiomegaly*, *lung opacity*, *lung lesion*, *edema*, *consolidation*, *pneumonia*, *atelectasis*, *pneumothorax*, *pleural effusion*, *pleural other*, *fracture*, *support devices*, and *no finding*.

positive results, and observations that are *negative*, *uncertain*, or *no mention* are all considered negative results. Following this, true positives, true negatives, and false negatives are found by comparing the observations of the generated reports to that of the ground truth reports. From this, the example-based precision, recall, and F-1 scores are found over the 14 observations, while the label-based precision, recall, and F-1 scores are found for each of the 14 observations [70, Section 7].

C. CXR pre-processing and augmentation

Following Chen *et al.*, we adopted the CXRs in JPEG and PNG formats for MIMIC-CXR and IU X-Ray, respectively, resulting in an 8-bit pixel depth and three identical channels ($C = 3$) [42]. This was required as each CV checkpoint was configured to take three channels as input (even CheXNet). The following pre-processing and augmentation steps were then applied to each CXR; first, a given CXR was resized using bilinear interpolation so that its smallest side had a length

of $W + 64$, where W is given in Table III, and its largest side was set such that it maintained the aspect ratio. Next, the resized CXR was cropped to a size of $\mathbb{R}^{3 \times W \times H}$, where $W = H$. The crop location was random during training and centered during testing. After this and only during training, the CXR was rotated around its centre where the angle of rotation was sampled from $\mathcal{U}[-5^\circ, 5^\circ]$. Finally, the CXR was standardised using the mean and standard deviation of each channel provided with each CV checkpoint.

D. Report pre-processing and generation

In order to compare to previous CXR report generators, we formatted the ground truth reports identically to Chen *et al.* [42]. This was achieved by including only the findings section of each ground truth report, allowing a maximum of 60 words per report (words after the 60th word were removed), changing upper-cased letters to lowercase, removing special characters, and replacing words that occurred less than three times in the corpus with a special unknown token. During testing, the maximum amount of subwords that the decoder could generate was set to 128, as each word could be represented by multiple subwords. Beam search with a beam size of four was used during testing when generating the reports. During validation and when generating the baseline for SCST, a beam size of one was used (i.e., greedy search).

E. Fine-tuning

Teacher forcing was used for fine-tuning [71]. When indicated, SCST was performed as an additional fine-tuning step after teacher forcing [39]. Each model was implemented in PyTorch version 1.9.0 and trained with 4×NVIDIA P100 16GB GPUs. To reduce memory consumption, we employed half precision (16-bit floating point) instead of full precision (32-bit floating point). To select the best epoch for a model, we use the highest CIDEr validation score. Due to phenomena such as mild overparameterisation, not every random initialisation of a models parameters will lead to a global minimum during gradient descent [72]. This leads to large performance variability between training runs. To account for this, we performed multiple training runs for each model. Finally, only models fine-tuned on the MIMIC-CXR training set were tested on the MIMIC-CXR test set and models fine-tuned on the IU X-Ray training set were tested on the IU X-Ray test set. The two stages of fine-tuning considered were:

1) *Teacher Forcing*: The following configuration was used to fine-tune each model with teacher forcing:

- Categorical cross-entropy as the loss function.
- *AdamW* optimiser [73] for gradient descent optimisation. An initial learning rate of $1e-5$ and $1e-4$ for the encoder and all other parameters, respectively, following Chen *et al.* [42]. All other hyperparameters for *AdamW* were set to their defaults.
- A mini-batch size of 16.
- Early stopping with a patience of 10 epochs and a minimum delta of $1e-4$.

- The validation CIDEr score was the monitored metric for early stopping.

2) *Self-Critical Sequence Training (SCST)*: The following configuration was used to further fine-tune designated models with SCST after teacher forcing:

- CIDEr as the reward.
- Stochastic Gradient Descent (SGD) with a learning rate of $1e-6$ and $1e-5$ for the encoder and all other parameters, respectively.
- A mini-batch size of 4.
- One epoch of SCST was performed for MIMIC-CXR.
- 10 epochs of SCST were performed for IU X-Ray.

F. Statistical analysis

The Confidence Intervals (CIs) in Tables V, VI, and VII were found with bootstrapping; the test set was resampled with replacement 1,000 times, where the size of each sample was equal to the size of the respective test set (as indicated in Table I) [74]. The 95% CIs were then calculated from the mean scores of each sample. In Subsections VI-D, VI-E, and VI-F we perform statistical tests on the NLG metric scores where the checkpoint type was the factor and the scores for each example of the MIMIC-CXR test set and for each of the training runs were the dependent variables. For each test, we used a *p*-value of 0.05. First, a Levene's test revealed that the variances of the scores were not homogeneous. This lead us to using a one-way Welch's ANOVA to determine if there was a significant difference between the scores of the checkpoints. If a significant difference existed, Games-Howell tests were used to perform a post hoc analysis.

VI. RESULTS AND DISCUSSION

In this section, we first compare the final model shown in Figure 4, whose encoder and decoder is warm-started with the CvT-21 ImageNet-21K and DistilGPT2 checkpoints, respectively, (i.e., CvT-212DistilGPT2) to current CXR report generators in the literature (Subsection VI-A). Next, we evaluate the diagnostic performance of CvT-212DistilGPT2 on 14 observations (Subsection VI-B). Following this, the case study in Subsection VI-C provides insight as to how CvT-212DistilGPT2 interprets a CXR when generating a report. In Subsection VI-D, we compare the CV checkpoints and determine which is best for warm-starting the encoder. Moreover, we compare the NLP checkpoints in Subsection VI-E and determine which is best for warm-starting the decoder. We also answer RQ1-RQ4 in Subsections VI-D and VI-E. Finally, we provide the reader with several future recommendations.

A. Comparison to current methods

Here, we compare CvT-212DistilGPT2 to other CXR report generators in the literature.⁴ The NLG metric scores on the MIMIC-CXR test set are shown in Table V. CvT-212DistilGPT2 attained the highest mean scores for all NLG

⁴Scores for the other CXR report generators in the literature were taken from their respective articles.

TABLE V

MEAN NLG AND EXAMPLE-BASED CE METRIC SCORES ON THE MIMIC-CXR TEST SET WITH THE LABELS OF CHEN *et al.* [42]. THE HIGHEST MEAN SCORE FOR EACH METRIC IS IN BOLDFACE. IF AVAILABLE, THE 95% CONFIDENCE INTERVALS ARE REPORTED. $n = 5$ INDICATES THE MEAN OVER FIVE TRAINING RUNS. * IS THE TRAINING RUN THAT SCORED THE HIGHEST VALIDATION CIDEr SCORE.

Model	Natural language generation metrics						Example-based CE metrics			
	BLEU-1	BLEU-2	BLEU-3	BLEU-4	METEOR	ROUGE-L	CIDEr	Precision	Recall	F-1
Transformer [42]	0.3140	0.1920	0.1270	0.0900	0.1250	0.2650	-	0.3310	0.2240	0.2280
R2Gen [42]	0.3530	0.2180	0.1450	0.1030	0.1420	0.2770	-	0.3330	0.2730	0.2760
CMN [43]	0.3530	0.2180	0.1480	0.1060	0.1420	0.2780	-	0.3340	0.2750	0.2780
Contrastive Attention [47]	0.3500	0.2190	0.1520	0.1090	0.1510	0.2830	-	0.3520	0.2980	0.3030
PPKED [48]	0.3600	0.2240	0.1490	0.1060	0.1490	0.2840	-	-	-	-
\mathcal{M}^2 Transformer Prog. [49]	0.3780	0.2320	0.1540	0.1070	0.1450	0.2720	-	0.2400	0.4280	0.3080
CvT-212DistilGPT2 ($n=5$)	0.3918 ± 0.00008	0.2454 ± 0.00008	0.1685 ± 0.00008	0.1236 ± 0.00009	0.1525 ± 0.00004	0.2846 ± 0.00007	0.3614 ± 0.00052	0.3597 ± 0.0003	0.4122 ± 0.0003	0.3842 ± 0.0002
CvT-212DistilGPT2* + SCST (CIDEr reward)	0.3928 ± 0.00013	0.2478 ± 0.00013	0.1713 ± 0.00013	0.1267 ± 0.00013	0.1545 ± 0.00007	0.2863 ± 0.00012	0.3892 ± 0.00077	0.3670 ± 0.0004	0.4184 ± 0.0004	0.3910 ± 0.0004
	0.3948 ± 0.00013	0.2490 ± 0.00013	0.1720 ± 0.00013	0.1272 ± 0.00013	0.1551 ± 0.00007	0.2878 ± 0.00012	0.3790 ± 0.00077	0.3653 ± 0.0004	0.4183 ± 0.0004	0.3900 ± 0.0004

TABLE VI

MEAN NLG METRIC SCORES ON THE IU X-RAY TEST SET WITH THE LABELS OF CHEN *et al.* [42]. THE HIGHEST MEAN SCORE FOR EACH METRIC IS IN BOLDFACE. IF AVAILABLE, THE 95% CONFIDENCE INTERVALS ARE REPORTED. $n = 5$ INDICATES THE MEAN OVER FIVE TRAINING RUNS. * IS THE TRAINING RUN THAT SCORED THE HIGHEST VALIDATION CIDEr SCORE.

Model	Natural language generation metrics						
	BLEU-1	BLEU-2	BLEU-3	BLEU-4	METEOR	ROUGE-L	CIDEr
Transformer [42]	0.3960	0.2540	0.1790	0.1350	0.1640	0.3420	-
R2Gen [42]	0.4700	0.3040	0.2190	0.1650	0.1870	0.3710	-
CMN [43]	0.4750	0.3090	0.2220	0.1700	0.1910	0.3750	-
Contrastive Attention [47]	0.4920	0.3140	0.2220	0.1690	0.1930	0.3810	-
PPKED [48]	0.4830	0.3150	0.2240	0.1680	0.1900	-	0.3510
\mathcal{M}^2 Transformer Progressive [49]	0.4860	0.3150	0.2240	0.1690	0.1920	0.3730	-
CvT-212DistilGPT2 ($n = 5$)	0.4620 ± 0.00038	0.2945 ± 0.00030	0.2141 ± 0.00030	0.1650 ± 0.00031	0.1924 ± 0.00022	0.3703 ± 0.00024	0.5868 ± 0.00335
CvT-212DistilGPT2* + SCST (CIDEr reward)	0.4732 ± 0.00045	0.3039 ± 0.00056	0.2242 ± 0.00061	0.1754 ± 0.00065	0.1997 ± 0.00029	0.3758 ± 0.00045	0.6935 ± 0.00495
	0.4777 ± 0.00044	0.3080 ± 0.00054	0.2274 ± 0.00060	0.1773 ± 0.00064	0.2032 ± 0.00028	0.3770 ± 0.00044	0.6814 ± 0.00483

metrics. Subsequently fine-tuning with SCST provided a small boost in performance for each NLG metric except for CIDEr—an anomaly as it was the reward. This indicates that the reports generated by CvT-212DistilGPT2 are more similar to the reports produced by radiologists than those of previous approaches.

For the example-based CE scores in Table V, \mathcal{M}^2 Transformer Progressive had the highest recall—but also the lowest precision. The authors of \mathcal{M}^2 Transformer Progressive speculated that the high false positive rate was due to its generated reports having a longer length on average than the ground truth reports [49, Section 4]. CvT-212DistilGPT2 was able to attain the highest precision and the second highest recall—leading to the highest F-1 score. This indicates that CvT-212DistilGPT2 is more diagnostically accurate than previous approaches.

The NLG metric scores on the IU X-Ray test set are shown in Table VI. CvT-212DistilGPT2 attained the highest mean scores for BLEU-3, BLEU-4, METEOR, and CIDEr. However, Contrastive Attention attained the highest mean BLEU-1 and ROUGE-L scores, while PPKED and \mathcal{M}^2 Transformer Progressive both attained the highest mean BLEU-2 score. This could indicate that the training set size of IU X-Ray is too small for CvT-212DistilGPT2. Alternatively, concatenating the visual features of the two CXRs—as shown in Figure 2 (right)—may not be the best multi-source combination technique, in fact, Libovicky *et al.* found it to be the worst technique for a Transformer decoder [75].

B. Performance on different observations

Next, to get an indication of the diagnostic accuracy of CvT-212DistilGPT2 for different abnormalities, we analyse its performance on each of the 14 CheXpert observations. Scores for the label-based CE metrics are given in Table VII, along with the macro- and micro-averaged scores over the observations. CvT-212DistilGPT2 attained the highest precision and recall for *support devices*—which is expected as it was one of the most frequent observations in the training set. CvT-212DistilGPT2 performed well for *pleural effusion* and *cardiomegaly*, of which both are frequently observed in the training set. For *no finding*, CvT-212DistilGPT2 demonstrated high precision but poor recall. Oppositely, it had a high recall and low precision for *lung opacity*. The performance of CvT-212DistilGPT2 for *consolidation*, *enlarged cardiomediastinum*, *lung lesion*, *fracture*, and *pleural other* was poor—likely due to the infrequency of these observations in the training set. This was also the case with previous CXR report generators, for example, the approach by Liu *et al.* performed poorly on the rarer abnormalities of MIMIC-CXR [37, Table 3]. This suggests that the class imbalance of the observations in the MIMIC-CXR training set leads to poor performance. Interestingly, recall was higher for all observations except *no finding* and *support devices*, as reflected by the macro- and micro-averaged scores for precision and recall. This shows that CvT-212DistilGPT2 has a higher false positive rate but a

lower false negative rate.

TABLE VII

LABEL-BASED CE METRIC SCORES OF CvT-212DistilGPT2 + SCST (CIDEr REWARD) FOR EACH OBSERVATION ON THE MIMIC-CXR TEST SET FROM CHEN *et al.* [42]. THE 95% CONFIDENCE INTERVALS ARE REPORTED FOR THE AVERAGED SCORES. THE POSITIVE OBSERVATION COUNT FOR THE TRAINING SET IS FROM [63, TABLE 2]. THE POSITIVE OBSERVATION COUNT FOR THE TEST SET OF CHEN *et al.* [42] WAS FOUND WITH CHEXBERT [69].

Observation	Count		CvT-212DistilGPT2 + SCST		
	Train set	Test set	Precision	Recall	F-1
No Finding	75,163	323	0.681	0.173	0.276
Support Devices	65,637	1,345	0.795	0.734	0.763
Pleural Effusion	53,188	1,056	0.454	0.692	0.548
Lung Opacity	50,916	1,392	0.227	0.551	0.321
Atelectasis	45,088	841	0.306	0.388	0.342
Cardiomegaly	39,094	1,271	0.512	0.591	0.549
Edema	26,455	563	0.224	0.468	0.303
Pneumonia	15,769	165	0.097	0.296	0.146
Consolidation	10,487	176	0.063	0.239	0.099
Pneumothorax	9,317	75	0.133	0.455	0.206
Enlarged Cardio.	7,004	320	0.066	0.093	0.077
Lung Lesion	6,129	199	0.010	0.167	0.019
Fracture	3,768	148	0.007	0.333	0.013
Pleural Other	1,961	122	0.016	0.167	0.030
Macro-averaged	-	-	0.256 \pm 0.0013	0.382 \pm 0.0003	0.307 \pm 0.0006
Micro-averaged	-	-	0.398 \pm 0.0004	0.497 \pm 0.0004	0.442 \pm 0.0003

C. Case study

Here, we observe the attention weights of a subset of the cross-attention heads of CvT-212DistilGPT2 as they collectively generate a word or subword for the case study in Figure 5. This case study was selected to highlight both strengths and weaknesses of the model and of the current paradigm of CXR report generators. It should be noted that higher layers (e.g., Layer 6) are considered higher-level representations of lower layers (e.g., Layer 1)—which typically model more primitive relationships. Because we are interested in the anatomical aspects of the CXR, we direct the readers attention to the higher layers.

Comparing the generated and ground truth reports, CvT-212DistilGPT2 correctly predicted that the patient has had Coronary Artery Bypass Graft (CABG) surgery via a median sternotomy incision, although it is unclear from both the generated and ground truth reports which of the coronary arteries were bypassed. It can be seen that the heads attended to the vascular clips when generating the subword ‘cab’—a key indicator of CABG. Next, CvT-212DistilGPT2 correctly identified the left-side pacemaker with its leads terminating in the right atrium and ventricle. Note that in the ground truth report, it was mentioned that the positioning of the leads remained ‘unchanged’—something that is impossible for CvT-212DistilGPT2 to infer as it has not observed the previous imaging session. It can be seen that Head 12 of Layer 6 and Head 1 of Layer 1 attend to the pacemaker when generating the subword ‘pac’|. However, not one of the presented heads attend to the lead in the right atrium when generating the subword ‘|rium’.

CvT-212DistilGPT2 indicated mild cardiomegaly with the phrase “a moderate enlargement of the cardiac silhouette”. However, CvT-212DistilGPT2 specified that the mild cardiomegaly was unchanged, referring to a previous, unobserved imaging session. This is because CvT-212DistilGPT2 has learnt to often describe abnormalities in the context of disease progression due to the ground truth reports of the training set frequently referring to previous imaging sessions. When generating the word ‘silhouette’, Head 6 of Layers 4 and 5 attend to regions of the cardiac silhouette. Moreover, CvT-212DistilGPT2 missed the widened and decreased curvature of the aortic arch indicating that the aorta is unfolded. CvT-212DistilGPT2 also mentioned that the mediastinal and hilar contours are similar, which is not a valid interpretation due to the word *similar*. Not one of the heads in Figure 5 attends to the right or left hilar points when generating the word ‘hilar’.

CvT-212DistilGPT2 also incorrectly predicted no pulmonary vascular congestion, while it is reported as mild and an improvement over a previous imaging session in the ground truth report. Head 7 of Layer 3 does pay some attention to the pulmonary vessels when generating the subword ‘cul’. However, it is difficult to determine an increased prominence of the pulmonary vessels without a prior normal CXR of the patient. Lastly, CvT-212DistilGPT2 mentions which abnormalities were not present in the CXR; no focal consolidation, pleural effusion, or pneumothorax. Some of the presented heads attend to regions of the pleura when generating the subword ‘|usion’, especially Head 6 of Layer 5. When looking for signs of pneumothorax, the heads did not attend to the position of the trachea, however, some attention was paid to each of the hemidiaphragms.

D. Best checkpoint for warm-starting the encoder

In this subsection, we determine which CV checkpoint is best for warm-starting the encoder. To succeed, the pre-training task of the CV checkpoint must be transferable to that of extracting salient visual features from CXRs. To make this investigation more tractable, the following methodology was adopted; for training, we use the 50K subset of MIMIC-CXR’s training set described in Subsection VI-F; SCST was not performed after teacher forcing; we make the assumption that the best CV checkpoint is independent of the NLP checkpoint used to warm-start the decoder. Following this, the decoder of each encoder-to-decoder model is warm-started with DistilGPT2. Eight training runs are performed for each CV checkpoint to account for the variability introduced by randomly initialising the parameters of P and the cross-attention modules of the decoder. The scores for the NLG metrics are shown in Figure 6, while the label-based CE metrics are shown in Figure 7. A one-way Welch’s ANOVA revealed a statistically significant difference between the NLG metric scores of each CV checkpoint, showing that they have an effect on performance.

CvT-13 attained the highest mean BLEU-4 score; CvT-21 the highest mean METEOR and CIDEr scores; BEiT the highest mean ROUGE-L score; ResNet-101 the highest macro-

Ground truth

patient is status post median sternotomy and cabg. left-sided pacemaker device is noted with leads terminating in the right atrium and right ventricle unchanged. the heart remains mildly enlarged but stable. the aorta is unfolded. there is mild pulmonary vascular congestion which is improved when compared to the prior exam. no new focal consolidation

Generated

the patient is status post median sternotomy and cabg. left-sided pacemaker device is noted with leads terminating in the right atrium and right ventricle. moderate enlargement of the cardiac silhouette is unchanged. the mediastinal and hilar contours are similar. pulmonary vasculature is not engorged. no focal consolidation pleural effusion or pneumothorax is present

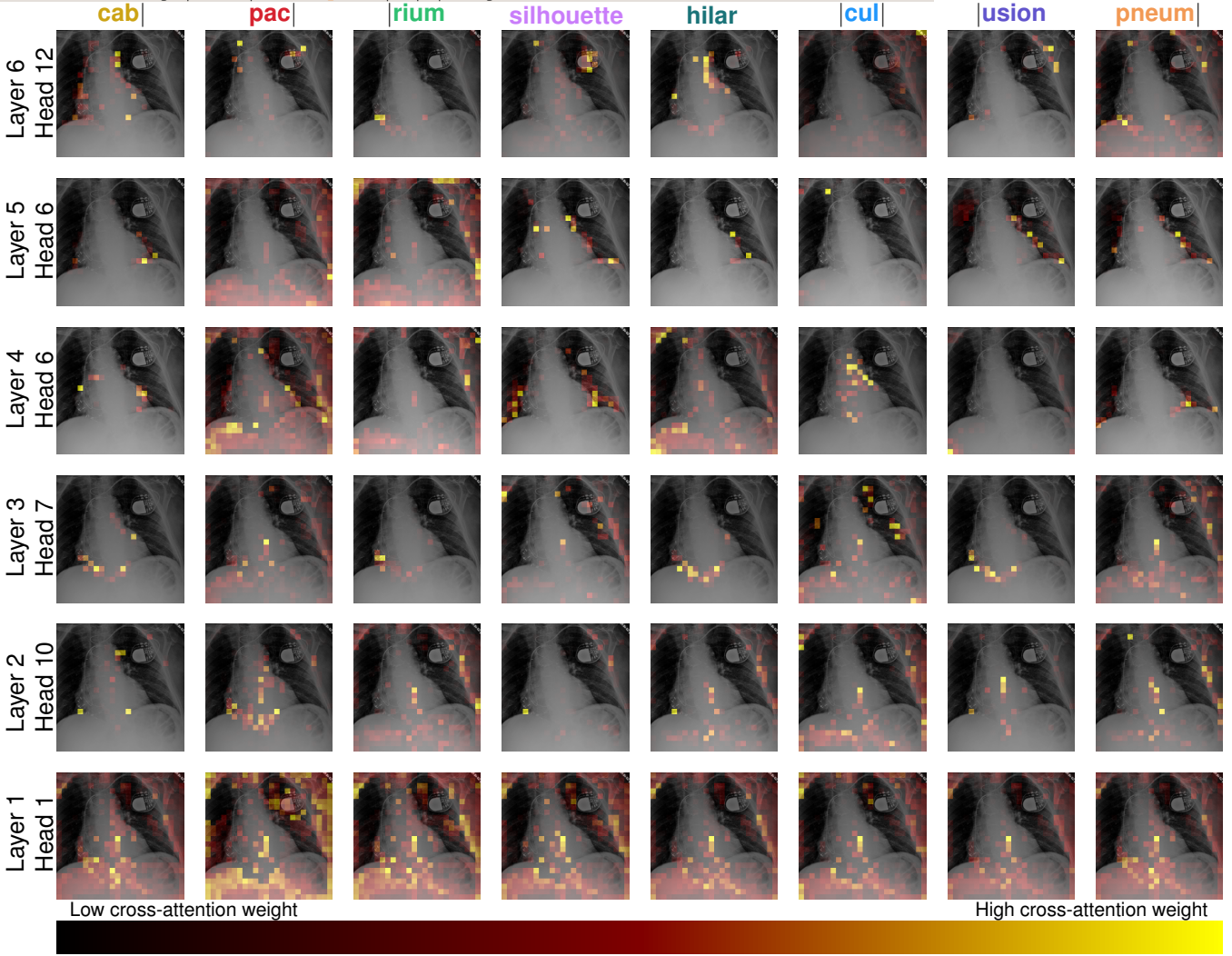


Fig. 5. Case study of CXR *a0578edb-12a640ca-1ddab351-089c4d4c-00bb6f19* from imaging session *s54265960* of patient *p18615099* from the MIMIC-CXR test set. The ‘ground truth’ report was produced by a radiologist, while the ‘generated’ report was produced by CvT-212DistilGPT2 + SCST (CIDEr reward). The CXR displayed has been pre-processed for testing. Subwords produced by DistilGPT2 are separated by a vertical bar. Each cross-attention weight matrix is min-max normalised and then scaled element wise using $\exp(1 - (1/\cdot))$ for ease of interpretation. A beam size of one (i.e., a greedy search) was used to produce the report. One cross-attention head from each layer of DistilGPT2 was selected for analysis.

averaged precision; DeiT the highest macro-averaged recall and micro-averaged precision and recall. Between the two best performing checkpoints, namely, CvT-21 and DeiT, CvT-21 attained higher mean BLEU-4, METEOR, ROUGE-L, CIDEr, and macro-averaged precision scores, while DeiT achieved

a higher macro-averaged recall and micro-averaged precision and recall. However, Games-Howell tests revealed no significant difference between their NLG metric scores. As CvT-21 and DeiT cannot be separated based on their performance, we instead select based on their parameter efficiency. Hence,

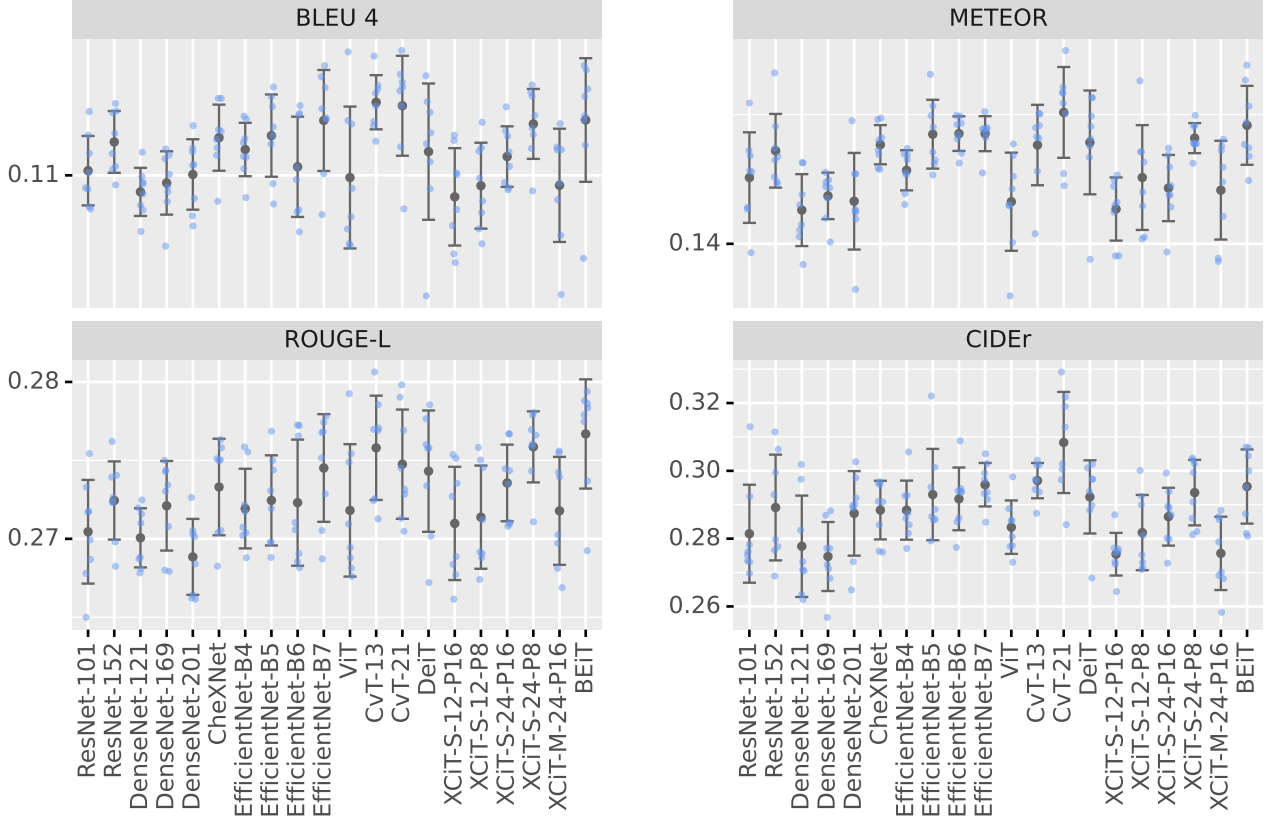


Fig. 6. NLG metric scores for each CV checkpoint when warm-starting the encoder. DistilGPT2 was used to warm-start the decoder. The black dots and the error bars indicate the mean and standard deviation over the training runs, respectively.

we select CvT-21 over DeiT as it consumes drastically fewer parameters (31.6M vs. 86M).

Comparing the CNN ImageNet-1K checkpoints, EfficientNet (B6 and B7) attained the highest scores for each metric (except for macro-averaged precision). In fact, Games-Howell tests revealed a significant difference between the METEOR scores of EfficientNet-B7 and each of the DenseNets. This is likely due to the improvements proposed by Tan *et al.* to scale the depth, width, and input image size of the network to more efficiently use the networks parameters [26]. Next, we compare the DenseNet-121 ImageNet-1K checkpoint to its domain-specific equivalent, namely CheXNet. CheXNet demonstrates a marked improvement, attaining higher mean scores for all metrics with Games-Howell tests revealing a statistically significant difference between their NLG metric scores.

Answer to RQ4 (for CV checkpoints): CheXNet demonstrates that there is a clear advantage to warm-starting the encoder with a domain-specific CV checkpoint over a general-domain CV checkpoint.

ViT lacked performance, attaining lower mean scores for all metrics (except macro-averaged precision) than EfficientNet-B5, B6, and B7. Moreover, Games-Howell tests confirmed a significant difference between the METEOR scores of EfficientNet-B5, B6, and B7 versus ViT. Its hard to pinpoint

the cause of the performance difference as many variables exist, such as the number of parameters and the training dataset. Another reason could be due to ViTs inability to model intra-patch visual features with its self-attention weights. The performance of DeiT was on par with EfficientNet, with DeiT attaining a higher macro- and micro-averaged precision and recall than EfficientNet-B7, whereas EfficientNet-B7 attained higher mean BLEU-4, METEOR, ROUGE-L, and CIDEr scores. Additionally, Games-Howell tests revealed no significant difference between the NLG metric scores of the two. The performance of BEiT was also on par with EfficientNet, with BEiT attaining higher mean BLEU-4, METEOR, ROUGE-L, and micro-averaged precision than EfficientNet-B7, whereas EfficientNet-B7 attained higher CIDEr, macro-averaged precision and recall, and micro-averaged recall. Moreover, Games-Howell tests revealed a significant difference between only the ROUGE-L scores of BEiT and EfficientNet-B4, B5, and B6 (in favour of BEiT), but not for B7. While having a similar architecture to ViT, the pre-training tasks of DeiT and BEiT enable them to perform comparatively to EfficientNet.

Finally, we analyse adaptations of the Transformer, namely XCiT and CvT. XCiT-S-24-P8 attained higher mean ROUGE-L and CIDEr scores than the EfficientNets, as well as a higher macro- and micro-averaged precision. However,

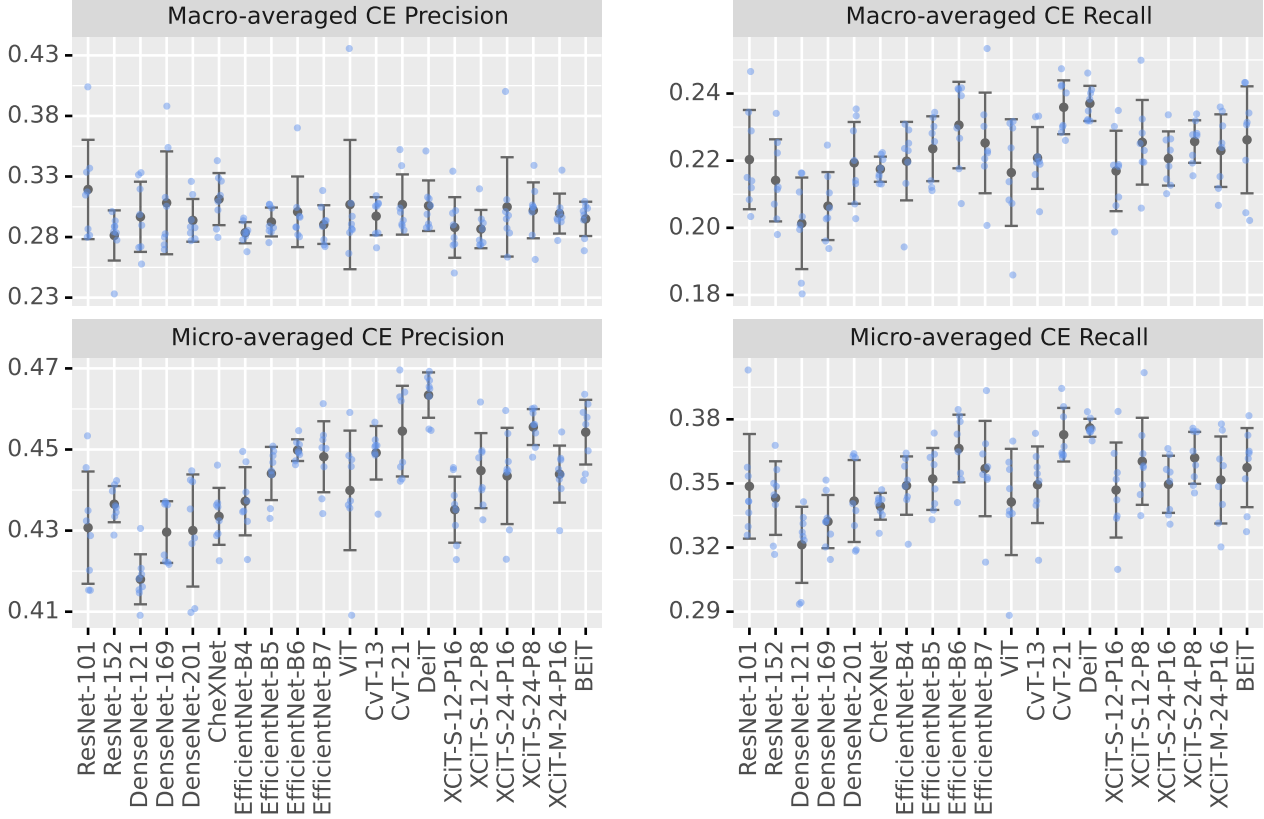


Fig. 7. Label-based CE scores for each CV checkpoint when warm-starting the encoder. DistilGPT2 was used to warm-start the decoder. The black dots and the error bars indicate the mean and standard deviation over the training runs, respectively.

Games-Howell tests only revealed significant difference for ROUGE-L between EfficientNet (B4, B5, and B6), but not for B7 (in favour of XCiT-S-24-P8). Moreover, EfficientNet-B6 and B7 attained higher mean BLEU-4 and METEOR scores as well as a higher macro- and micro-averaged recall. CvT-21 attained higher mean scores than the EfficientNets for all metrics, indicating that CvT-21 is the only Transformer-based CV checkpoint that can consistently outperform EfficientNet. However, Games-Howell tests revealed no statistically significant difference between the NLG metric scores of EfficientNet-B7 and CvT-21.

Answer to RQ1: Currently, it seems that Transformers require pre-training with a task such as MIM or distillation to perform comparatively to CNNs. However, the performance of CvT suggests that incorporating convolutional layers into the Transformer alleviates it from having to learn the inductive bias of local spatial feature processing, allowing it to outperform EfficientNet.

E. Best checkpoint for warm-starting the decoder

This subsection is identical in methodology to the previous subsection, except that now we determine which NLP checkpoint is best for warm-starting the decoder. A ResNet-101 ImageNet-1K checkpoint was employed to warm-start the encoder of each encoder-to-decoder model following the

assumption that the best NLP checkpoint is independent of the CV checkpoint used to warm-start the encoder. To succeed, the pre-training task of an NLP checkpoint must be transferable to that of generating reports from visual features. The scores for the NLG metrics are shown in Figure 8, while the label-based CE metrics are shown in Figure 9. A one-way Welch’s ANOVA revealed a statistically significant difference between the NLG metric scores of each checkpoint, showing that they have an effect on performance.

DistilGPT2 attained the highest mean BLEU-4, METEOR, ROUGE-L, and CIDEr scores while GPT2 attained the highest macro-averaged recall and micro-averaged precision and recall. Furthermore, Games-Howell tests revealed a statistically significant difference between the scores of both GPT2 and DistilGPT2 versus the remaining checkpoints for both METEOR and CIDEr, indicating that GPT2 and DistilGPT2 are the most suitable checkpoints for warm-starting the decoder. Comparing GPT2 to DistilGPT2, Games-Howell tests revealed no significant difference between their NLG metric scores, showing that distilling GPT2 to 66% of its parameters has no effect on performance.⁵ Due to its parameter efficiency,

⁵Games-Howell tests also revealed no significant difference between the NLG metric scores of BERT and DistilBERT, again demonstrating that distillation does not impact performance.

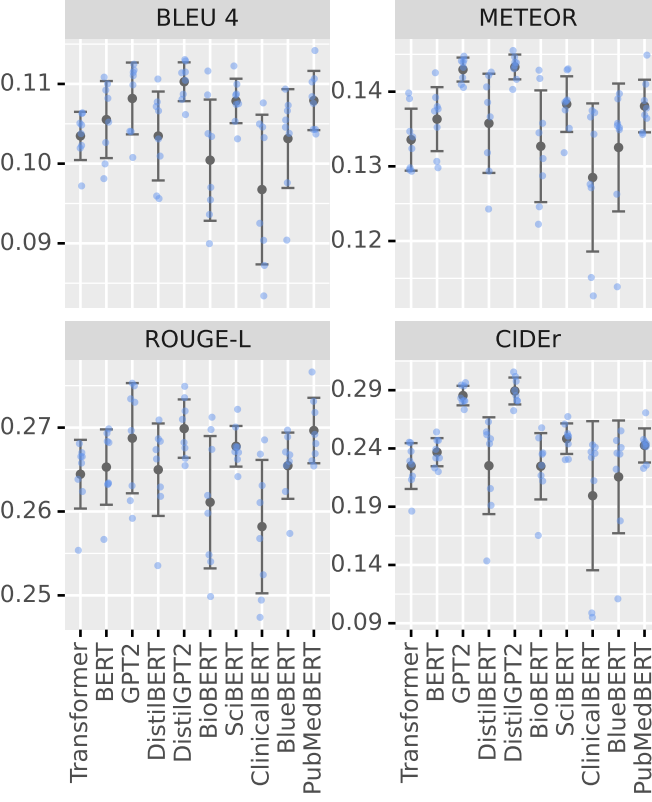


Fig. 8. NLG metric scores for each NLP checkpoint when warm-starting the decoder. A ResNet-101 ImageNet-1K checkpoint was used to warm-start the encoder. The black dots and the error bars indicate the mean and standard deviation over the training runs, respectively.

we select DistilGPT2 over GPT2 as the best checkpoint for warm-starting the decoder.

Answer to RQ2: GPT2 demonstrated that an NLP checkpoint can be effectively fine-tuned to model not only natural language, but also visual features (i.e., a pre-trained NLP checkpoint is able to outperform a randomly initialised decoder).

Comparing BERT and GPT2, Games-Howell tests revealed a significant difference between their METEOR, ROUGE-L, and CIDEr scores (in favour of GPT2). GPT2 also attained higher label-based CE scores than BERT. This finding is opposite to that of Rothe *et al.* [33, BERT2BERT vs. BERT2GPT2]; however, the encoder in their case was an NLP checkpoint rather than a CV checkpoint. Some of the main differences between BERT and GPT2 include their number of parameters (110M for BERT vs. 124M for GPT2), their training data (BookCorpus and English Wikipedia for BERT vs. WebText for GPT2), their vocabulary size and source (30K formed from BookCorpus and English Wikipedia for BERT vs. 50K formed from WebText for GPT2), and their token embeddings (BERT uses WordPiece [31] while GPT2 uses byte-pair encodings [32]). However, we hypothesise that these differences are relatively minor and have only a slight effect on the performance difference. Instead, we speculate that their pre-training tasks

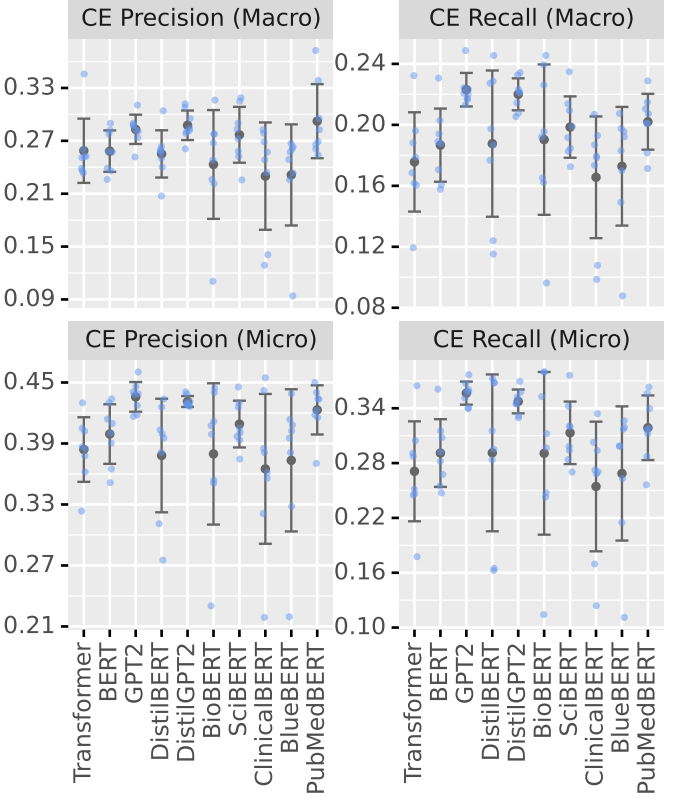


Fig. 9. Label-based CE scores for each NLP checkpoint when warm-starting the decoder. A ResNet-101 ImageNet-1K checkpoint was used to warm-start the encoder. The black dots and the error bars indicate the mean and standard deviation over the training runs, respectively.

are the main cause of the performance difference and suggest that GPT2’s language modelling pre-training task is better than BERT’s MLM and NSP pre-training tasks for CXR report generation.

Answer to RQ3: GPT2 is able to outperform BERT. Our hypothesis as to why this is the case is due to their different pre-training tasks (MLM and NSP vs. language modelling).

Amongst the domain-specific NLU checkpoints, PubMedBERT performed best. Games-Howell tests revealed a significant difference between the METEOR and ROUGE-L scores of BERT and PubMedBERT (in favour of PubMedBERT). PubMedBERT also attained higher label-based CE metric scores. This indicates that a biomedical NLU checkpoint is better than a general-domain NLU checkpoint for warm-starting the decoder. Opposite to PubMedBERT, BioBERT lacked performance, with Games-Howell tests revealing a significant difference between all of the NLG metric scores of BioBERT and PubMedBERT (in favour of PubMedBERT). Additionally, PubMedBERT achieved higher label-based CE metric scores. Unlike BioBERT, PubMedBERT was pre-trained from scratch on PubMed and PMC and has a domain-specific vocabulary, both of which are cited as the reason why PubMedBERT outperforms BioBERT on biomedical NLU tasks [59].

For the EHR NLU checkpoints, BlueBERT was outperformed by both BERT and PubMedBERT, attaining lower mean scores for each metric (except for ROUGE-L, where BlueBERT attained a higher mean ROUGE-L score than BERT).⁶ Furthermore, Games-Howell tests revealed a significant difference between all the NLG metric scores of BlueBERT and PubMedBERT, and a significant difference between the METEOR and CIDEr scores of BlueBERT and BERT. Several factors could be causing the deficit in performance to the general-domain and biomedical NLU checkpoints. Unlike BERT or PubMedBERT, ClinicalBERT and BlueBERT are not pre-trained from scratch, rather, each involves three stages of pre-training, as shown in Table IV. Moreover, MIMIC-III is significantly smaller than the datasets used to pre-train BERT and PubMedBERT (Table I). Finally, both ClinicalBERT and BlueBERT do not have domain-specific vocabularies.

Answer to RQ4 (for NLP checkpoints): While PubMedBERT outperformed BERT, the ELU NLU checkpoints—which are closer in domain to CXR reports—did not. This is more likely due to factors other than the choice of domain, such as the size of the pre-training datasets and the use of domain-specific vocabularies.

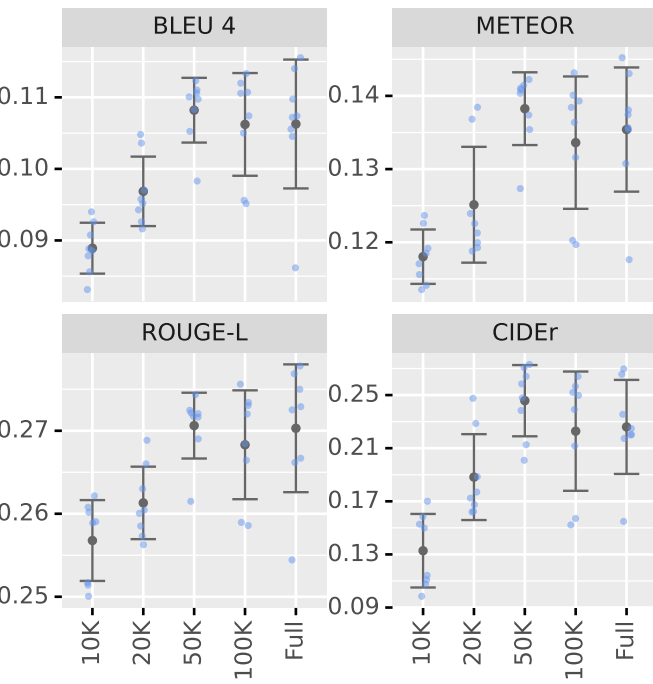


Fig. 10. Different subset sizes of MIMIC-CXR’s training set. ResNet-1012DistilBERT was used for the comparison. The black dots and the error bars indicate the mean and standard deviation over the training runs, respectively.

⁶BlueBERT outperformed ClinicalBERT, attaining higher mean scores for each metric, with Games-Howell tests revealing a significant difference between their NLG metric scores.

F. No. of training examples

In order to make the experiments in Subsections VI-D and VI-E tractable, we sought to find a subset size of the MIMIC-CXR training set that was large enough that it produced similar results to the full training set, yet small enough that a model would not take too long to train. Hence, we investigate different subset sizes of the MIMIC-CXR training set, as presented in Figure 10. For each size, each training run used the same random sample (without replacement) of the MIMIC-CXR training set. We selected ResNet-1012DistilBERT as the model. Eight training runs were conducted for each training size, where only teacher forcing was employed during fine-tuning. A one-way Welch’s ANOVA revealed a significant difference between the scores of each NLG metric over the different sizes. Games-Howell tests revealed a significant difference between the scores for 10K and 20K and the full training set. This was not the case with 50K and 100K and the full training set. Hence, we use the 50K subset of MIMIC-CXR’s training set in Subsections VI-D and VI-E, as it is the smallest tested size with no statistically significant difference to the full training set.

VII. FUTURE RECOMMENDATIONS

There are several recommendations we propose for future investigation:

- 1) CXRs in DICOM format—as they have a 12-bit pixel depth rather than 8-bit. The reduction in quantisation error could improve performance.
- 2) Downsampling each CXR to 384×384 increases the risk of missing fine details. Hence, the downsampled CXR should be closer in resolution to the original CXR. However, this is more difficult to implement than increasing the pixel depth—as the CV model would need to be modified.
- 3) Current CXR report generators that are evaluated on MIMIC-CXR typically generate a report from only a single view of an imaging session. All available views should be used for an imaging session as certain abnormalities are easier to detect when interpreting both frontal and lateral views simultaneously.
- 4) Radiologists frequently reference previous imaging sessions of a patient in the ground truth reports. We hypothesise that observing both the generated reports and/or the visual features of previous imaging sessions will further improve CXR report generation. This will be especially important for monitoring disease progression.
- 5) Motivated by Section VI-B, we hypothesise that an under or over sampling technique could reduce the impact of the class imbalance of the MIMIC-CXR training set.
- 6) There also exists more recent CV checkpoints which are not yet open-source that may outperform CvT. For example, a ViT checkpoint was formed that had the image patches as input replaced with the output of a small number of stacked stride-two 3×3 convolutions (ViT_c). By injecting this inductive bias towards local

spatial feature processing, ViT_c is able to outperform ViT and EfficientNet [76].

- 7) As demonstrated by CheXNet outperforming the DenseNet-121 ImageNet-21K checkpoint, a domain-specific CvT-21 checkpoint may be more apt for warm-starting the encoder than the CvT-21 ImageNet-21K checkpoint.
- 8) This study indicates that the following modifications to DistilGPT2 checkpoint should be investigated: i) pre-training on PubMed and PMC from scratch before distillation, and ii) using a domain-specific vocabulary.
- 9) An important consideration is the level of diagnostic accuracy that a CXR report generator must attain before retrospective or prospective clinical trials are deemed appropriate. Understanding the diagnostic accuracy of humans will help establish this, for example, a study by Satia *et al.* found that the diagnostic accuracy of clinicians ranged from 66% to 83% depending on expertise [3, Table 1]. As demonstrated in Table VII, current CXR report generators demonstrate poor diagnostic accuracy for multiple abnormalities, indicating that further research and development is required before reaching such a threshold.
- 10) Metrics that evaluate the clinical decisions inferred from the generated reports should be considered—as clinical decisions ultimately dictate patient care.

VIII. CONCLUSION

In this study, we investigate warm-starting the encoder and decoder of a CXR report generator with recent open-source CV and NLP checkpoints. Our investigation led us to the CvT-21 ImageNet-21K checkpoint—which possesses the advantages of both CNNs and Transformers—as the best CV checkpoint for warm-starting the encoder. Moreover, we find that DistilGPT2—a distilled general-domain NLG checkpoint—is best for warm-starting the decoder. The results indicate that the reports generated by CvT-212DistilGPT2 are more diagnostically accurate and have a higher similarity to radiologist reports than previous approaches. Compared to \mathcal{M}^2 Transformer Progressive, CvT-212DistilGPT2 attained an improvement of 8.3% for CE F-1, 1.8% for BLEU-4, 1.6% for ROUGE-L, and 1.0% for METEOR.

Our investigation also reveals several important findings about warm-starting the encoder and decoder of a CXR report generator. The first is that a Transformer-based CV checkpoint that incorporates convolutional layers is better than a CNN checkpoint for warm-starting the encoder. Moreover, an NLP checkpoint can be effectively fine-tuned to model not only natural language but also visual features. Furthermore, we find that GPT2 is better for warm-starting the decoder than BERT. Finally, we found that domain-specific checkpoints are better for warm-starting than general-domain checkpoints—if the pre-training dataset is sufficient. In general, the best checkpoint for a task depends on multiple variables; for example, the pre-training task, the size and quality of the dataset, the vocabulary, and the model architecture.

By leveraging warm-starting, CvT-212DistilGPT2 brings automatic CXR report generation one step closer to the clinical setting. The future outlook on CXR report generation is promising; a CXR report generator that has been clinically validated through retrospective and prospective trials—that also meets regulatory requirements—could have a significant impact on radiology. Automatic CXR report generation could provide more consistent and reliable reporting, as well as cheaper running costs. It could also reduce the burden placed on overworked radiologists. A secondary use for such a technology could be to conduct a retrospective analysis on previous reports, which in turn could be used for other tasks such as question answering or population research. CvT-212DistilGPT2 and its MIMIC-CXR checkpoint are available at <https://github.com/aehrc/cvt2distilgpt2>.

REFERENCES

- [1] B. Kelly, “The chest radiograph,” *The Ulster medical journal*, vol. 81, no. 23620614, pp. 143–148, Sep. 2012. [Online]. Available: <https://www.ncbi.nlm.nih.gov/pmc/articles/PMC3632825/>
- [2] J. P. Kanne, N. Thoongsuwan, and E. J. Stern, “Common Errors and Pitfalls in Interpretation of the Adult Chest Radiograph,” *Clinical Pulmonary Medicine*, vol. 12, no. 2, pp. 97–114, mar 2005.
- [3] I. Satia, S. Bashagha, A. Bibi, R. Ahmed, S. Mellor, and F. Zaman, “Assessing the accuracy and certainty in interpreting chest X-rays in the medical division,” *Clinical Medicine*, vol. 13, no. 4, pp. 349–352, aug 2013.
- [4] R. J. McDonald, K. M. Schwartz, L. J. Eckel, F. E. Diehn, C. H. Hunt, B. J. Bartholmai, B. J. Erickson, and D. F. Kallmes, “The Effects of Changes in Utilization and Technological Advancements of Cross-Sectional Imaging on Radiologist Workload,” *Academic Radiology*, vol. 22, no. 9, pp. 1191–1198, sep 2015.
- [5] J. X. Liu, Y. Goryakin, A. Maeda, T. Bruckner, and R. Scheffler, “Global Health Workforce Labor Market Projections for 2030,” *Human Resources for Health*, vol. 15, no. 1, feb 2017.
- [6] J. A. Harolds, J. R. Parikh, E. I. Bluth, S. C. Dutton, and M. P. Recht, “Burnout of Radiologists: Frequency, Risk Factors, and Remedies: A Report of the ACR Commission on Human Resources,” *Journal of the American College of Radiology*, vol. 13, no. 4, pp. 411–416, apr 2016.
- [7] E. A. Krupinski, K. S. Berbaum, R. T. Caldwell, K. M. Schartz, and J. Kim, “Long Radiology Workdays Reduce Detection and Accommodation Accuracy,” *Journal of the American College of Radiology*, vol. 7, no. 9, pp. 698–704, sep 2010.
- [8] Y. Balabanova, R. Coker, I. Fedorin, S. Zakharova, S. Plavinskij, N. Krukov, R. Atun, and F. Drobnieowski, “Variability in interpretation of chest radiographs among Russian clinicians and implications for screening programmes: observational study,” *BMJ*, vol. 331, no. 7513, pp. 379–382, aug 2005.
- [9] “Good practice for radiological reporting. Guidelines from the European Society of Radiology (ESR),” *Insights into Imaging*, vol. 2, no. 2, pp. 93–96, feb 2011.
- [10] D. Siegal, L. M. Stratchko, and C. DeRoo, “The role of radiology in diagnostic error: a medical malpractice claims review,” *Diagnosis*, vol. 4, no. 3, pp. 125–131, sep 2017.
- [11] J. Vosshenrich, P. Brantner, J. Cyriac, D. T. Boll, E. M. Merkle, and T. Heye, “Quantifying radiology resident fatigue: Analysis of preliminary reports,” *Radiology*, vol. 298, no. 3, pp. 632–639, mar 2021.
- [12] J. Pavlopoulos, V. Kougia, I. Androultsopoulos, and D. Papamichail, “Diagnostic Captioning: A Survey,” *arXiv:2101.07299 [cs.CV]*, Jan. 2021.
- [13] J. H. Thrall, X. Li, Q. Li, C. Cruz, S. Do, K. Dreyer, and J. Brink, “Artificial Intelligence and Machine Learning in Radiology: Opportunities, Challenges, Pitfalls, and Criteria for Success,” *Journal of the American College of Radiology*, vol. 15, no. 3, pp. 504–508, mar 2018.
- [14] A. Alexander, A. Jiang, C. Ferreira, and D. Zurkiya, “An Intelligent Future for Medical Imaging: A Market Outlook on Artificial Intelligence for Medical Imaging,” *Journal of the American College of Radiology*, vol. 17, no. 1, pp. 165–170, jan 2020.

[15] K. G. V. Leeuwen, M. de Rooij, S. Schalekamp, B. van Ginneken, and M. J. C. M. Rutten, "How does artificial intelligence in radiology improve efficiency and health outcomes?" *Pediatric Radiology*, jun 2021.

[16] C. J. Kelly, A. Karthikesalingam, M. Suleyman, G. Corrado, and D. King, "Key challenges for delivering clinical impact with artificial intelligence," *BMC Medicine*, vol. 17, no. 1, oct 2019.

[17] K. He, X. Zhang, S. Ren, and J. Sun, "Deep Residual Learning for Image Recognition," in *2016 IEEE Conference on Computer Vision and Pattern Recognition (CVPR)*. IEEE, jun 2016.

[18] G. Huang, Z. Liu, L. V. D. Maaten, and K. Q. Weinberger, "Densely Connected Convolutional Networks," in *2017 IEEE Conference on Computer Vision and Pattern Recognition (CVPR)*. IEEE, jul 2017.

[19] A. Vaswani, N. Shazeer, N. Parmar, J. Uszkoreit, L. Jones, A. N. Gomez, u. Kaiser, and I. Polosukhin, "Attention is All You Need," in *Proceedings of the 31st International Conference on Neural Information Processing Systems*, ser. NIPS'17. Red Hook, NY, USA: Curran Associates Inc., 2017, p. 6000–6010.

[20] A. Ke, W. Ellsworth, O. Banerjee, A. Y. Ng, and P. Rajpurkar, "CheX-transfer: performance and parameter efficiency of ImageNet models for chest X-Ray interpretation," in *Proceedings of the Conference on Health, Inference, and Learning*. ACM, apr 2021, pp. 116–124.

[21] O. Russakovsky, J. Deng, H. Su, J. Krause, S. Satheesh, S. Ma, Z. Huang, A. Karpathy, A. Khosla, M. Bernstein, A. C. Berg, and L. Fei-Fei, "ImageNet Large Scale Visual Recognition Challenge," *International Journal of Computer Vision*, vol. 115, no. 3, pp. 211–252, apr 2015.

[22] O. Alfarqhal, R. Khaled, A. Elkorany, M. Helal, and A. Fahmy, "Automated radiology report generation using conditioned transformers," *Informatics in Medicine Unlocked*, vol. 24, p. 100557, 2021.

[23] A. Kolesnikov, L. Beyer, X. Zhai, J. Puigcerver, J. Yung, S. Gelly, and N. Houlsby, "Big Transfer (BiT): General Visual Representation Learning," in *Computer Vision – ECCV 2020*. Springer International Publishing, 2020, pp. 491–507.

[24] H. Bao, L. Dong, and F. Wei, "BEiT: BERT Pre-Training of Image Transformers," *arXiv:2106.08254 [cs.CV]*, Jun. 2021.

[25] H. Touvron, M. Cord, M. Douze, F. Massa, A. Sablayrolles, and H. Jegou, "Training data-efficient image transformers & distillation through attention," in *Proceedings of the 38th International Conference on Machine Learning*, ser. Proceedings of Machine Learning Research, M. Meila and T. Zhang, Eds., vol. 139. PMLR, 18–24 Jul 2021, pp. 10347–10357. [Online]. Available: <https://proceedings.mlr.press/v139/touvron21a.html>

[26] M. Tan and Q. Le, "EfficientNet: Rethinking Model Scaling for Convolutional Neural Networks," in *Proceedings of the 36th International Conference on Machine Learning*, ser. Proceedings of Machine Learning Research, K. Chaudhuri and R. Salakhutdinov, Eds., vol. 97. PMLR, 09–15 Jun 2019, pp. 6105–6114. [Online]. Available: <http://proceedings.mlr.press/v97/tan19a.html>

[27] A. Dosovitskiy, L. Beyer, A. Kolesnikov, D. Weissenborn, X. Zhai, T. Unterthiner, M. Dehghani, M. Minderer, G. Heigold, S. Gelly, J. Uszkoreit, and N. Houlsby, "An Image is Worth 16x16 Words: Transformers for Image Recognition at Scale," *arXiv:2010.11929 [cs.CV]*, Oct. 2020.

[28] H. Wu, B. Xiao, N. Codella, M. Liu, X. Dai, L. Yuan, and L. Zhang, "CVT: Introducing Convolutions to Vision Transformers," *arXiv:2103.15808 [cs.CV]*, Mar. 2021.

[29] A. El-Nouby, H. Touvron, M. Caron, P. Bojanowski, M. Douze, A. Joulin, I. Laptev, N. Neverova, G. Synnaeve, J. Verbeek, and H. Jegou, "XCiT: Cross-Covariance Image Transformers," *arXiv:2106.09681 [cs.CV]*, Jun. 2021.

[30] M. Naseer, K. Ranasinghe, S. Khan, M. Hayat, F. S. Khan, and M.-H. Yang, "Intriguing Properties of Vision Transformers," *arXiv:2105.10497 [cs.CV]*, May 2021.

[31] J. Devlin, M. Chang, K. Lee, and K. Toutanova, "BERT: Pre-training of Deep Bidirectional Transformers for Language Understanding," in *Proceedings of the 2019 Conference of the North American Chapter of the Association for Computational Linguistics: Human Language Technologies, Volume 1 (Long and Short Papers)*. Minneapolis, Minnesota: Association for Computational Linguistics, Jun. 2019, pp. 4171–4186. [Online]. Available: <https://www.aclweb.org/anthology/N19-1423>

[32] A. Radford, J. Wu, R. Child, D. Luan, D. Amodei, and I. Sutskever, "Language Models are Unsupervised Multitask Learners," 2019.

[33] S. Rothe, S. Narayan, and A. Severyn, "Leveraging Pre-trained Checkpoints for Sequence Generation Tasks," *Transactions of the Association for Computational Linguistics*, vol. 8, pp. 264–280, Dec. 2020.

[34] J. Lee, W. Yoon, S. Kim, D. Kim, S. Kim, C. H. So, and J. Kang, "BioBERT: a pre-trained biomedical language representation model for biomedical text mining," *Bioinformatics*, sep 2019.

[35] N. Kaur, A. Mittal, and G. Singh, "Methods for automatic generation of radiological reports of chest radiographs: a comprehensive survey," *Multimedia Tools and Applications*, sep 2021.

[36] X. Wang, Y. Peng, L. Lu, Z. Lu, and R. M. Summers, "TieNet: Text-Image Embedding Network for Common Thorax Disease Classification and Reporting in Chest X-Rays," in *2018 IEEE/CVF Conference on Computer Vision and Pattern Recognition*. IEEE, jun 2018.

[37] G. Liu, T. H. Hsu, M. McDermott, W. Boag, W. Weng, P. Szolovits, and M. Ghassemi, "Clinically Accurate Chest X-Ray Report Generation," in *Proceedings of the 4th Machine Learning for Healthcare Conference*, ser. Proceedings of Machine Learning Research, F. Doshi-Velez, J. Fackler, K. Jung, D. Kale, R. Ranganath, B. Wallace, and J. Wiens, Eds., vol. 106. Ann Arbor, Michigan: PMLR, 09–10 Aug 2019, pp. 249–269. [Online]. Available: <http://proceedings.mlr.press/v106/liu19a.html>

[38] J. Irvin, P. Rajpurkar, M. Ko, Y. Yu, S. Ciurea-Ilcus, C. Chute, H. Marklund, B. Haghgoor, R. Ball, K. Shpanskaya, J. Seekins, D. A. Mong, S. S. Halabi, J. K. Sandberg, R. Jones, D. B. Larson, C. P. Langlotz, B. N. Patel, M. P. Lungren, and A. Y. Ng, "CheXpert: A Large Chest Radiograph Dataset with Uncertainty Labels and Expert Comparison," vol. 33. Association for the Advancement of Artificial Intelligence (AAAI), jul 2019, pp. 590–597.

[39] S. J. Rennie, E. Marcheret, Y. Mroueh, J. Ross, and V. Goel, "Self-Critical Sequence Training for Image Captioning," in *2017 IEEE Conference on Computer Vision and Pattern Recognition (CVPR)*. IEEE, jul 2017.

[40] Y. Zhang, X. Wang, Z. Xu, Q. Yu, A. Yuille, and D. Xu, "When Radiology Report Generation Meets Knowledge Graph," *Proceedings of the AAAI Conference on Artificial Intelligence*, vol. 34, no. 07, pp. 12910–12917, Apr. 2020.

[41] J. Lovelace and B. Mortazavi, "Learning to Generate Clinically Coherent Chest X-Ray Reports," in *Findings of the Association for Computational Linguistics: EMNLP 2020*. Association for Computational Linguistics, Nov. 2020, pp. 1235–1243. [Online]. Available: <https://www.aclweb.org/anthology/2020.findings-emnlp.110>

[42] Z. Chen, Y. Song, T. Chang, and X. Wan, "Generating Radiology Reports via Memory-driven Transformer," in *Proceedings of the 2020 Conference on Empirical Methods in Natural Language Processing (EMNLP)*. Association for Computational Linguistics, 2020, pp. 1439–1449.

[43] Z. Chen, Y. Shen, Y. Song, and X. Wan, "Cross-modal Memory Networks for Radiology Report Generation," in *Proceedings of the 59th Annual Meeting of the Association for Computational Linguistics and the 11th International Joint Conference on Natural Language Processing (Volume 1: Long Papers)*. Association for Computational Linguistics, 2021.

[44] B. Jing, Z. Wang, and E. Xing, "Show, Describe and Conclude: On Exploiting the Structure Information of Chest X-ray Reports," in *Proceedings of the 57th Annual Meeting of the Association for Computational Linguistics*. Association for Computational Linguistics, 2019.

[45] C. Y. Li, X. Liang, Z. Hu, and E. P. Xing, "Hybrid Retrieval-Generation Reinforced Agent for Medical Image Report Generation," in *Proceedings of the 32nd International Conference on Neural Information Processing Systems*, ser. NIPS'18. Red Hook, NY, USA: Curran Associates Inc., 2018, p. 1537–1547.

[46] B. Jing, P. Xie, and E. Xing, "On the Automatic Generation of Medical Imaging Reports," in *Proceedings of the 56th Annual Meeting of the Association for Computational Linguistics (Volume 1: Long Papers)*. Association for Computational Linguistics, 2018.

[47] F. Liu, C. Yin, X. Wu, S. Ge, P. Zhang, and X. Sun, "Contrastive Attention for Automatic Chest X-ray Report Generation," in *Findings of the Association for Computational Linguistics: ACL-IJCNLP 2021*. Online: Association for Computational Linguistics, Aug. 2021, pp. 269–280. [Online]. Available: <https://aclanthology.org/2021.findings-acl.23>

[48] F. Liu, X. Wu, S. Ge, W. Fan, and Y. Zou, "Exploring and Distilling Posterior and Prior Knowledge for Radiology Report Generation," in

Proceedings of the IEEE/CVF Conference on Computer Vision and Pattern Recognition (CVPR), June 2021, pp. 13 753–13 762.

[49] F. Nooralahzadeh, N. P. Gonzalez, T. Frauenfelder, K. Fujimoto, and M. Krauthammer, “Progressive Transformer-Based Generation of Radiology Reports,” *arXiv:2102.09777 [cs.CL]*, Feb. 2021.

[50] M. Cornia, M. Stefanini, L. Baraldi, and R. Cucchiara, “Mesched-Memory Transformer for Image Captioning,” in *Proceedings of the IEEE/CVF Conference on Computer Vision and Pattern Recognition (CVPR)*, June 2020.

[51] M. Lewis, Y. Liu, N. Goyal, M. Ghazvininejad, A. Mohamed, O. Levy, V. Stoyanov, and L. Zettlemoyer, “BART: Denoising Sequence-to-Sequence Pre-training for Natural Language generation, translation, and comprehension,” in *Proceedings of the 58th Annual Meeting of the Association for Computational Linguistics*. Online: Association for Computational Linguistics, Jul. 2020, pp. 7871–7880. [Online]. Available: <https://aclanthology.org/2020.acl-main.703>

[52] P. Rajpurkar, J. Irvin, K. Zhu, B. Yang, H. Mehta, T. Duan, D. Ding, A. Bagul, C. Langlotz, K. Shpanskaya, M. P. Lungren, and A. Y. Ng, “CheXNet: Radiologist-Level Pneumonia Detection on Chest X-Rays with Deep Learning,” *arXiv:1711.05225 [cs.CV]*, Nov. 2017.

[53] Y. Zhu, R. Kiros, R. Zemel, R. Salakhutdinov, R. Urtasun, A. Torralba, and S. Fidler, “Aligning Books and Movies: Towards Story-Like Visual Explanations by Watching Movies and Reading Books,” in *Proceedings of the IEEE International Conference on Computer Vision (ICCV)*, December 2015.

[54] V. Sanh, L. Debut, J. Chaumond, and T. Wolf, “DistilBERT, a distilled version of BERT: smaller, faster, cheaper and lighter,” *arXiv:1910.01108 [cs.CL]*, Oct. 2019.

[55] I. Beltagy, K. Lo, and A. Cohan, “SciBERT: A Pretrained Language Model for Scientific Text,” in *Proceedings of the 2019 Conference on Empirical Methods in Natural Language Processing and the 9th International Joint Conference on Natural Language Processing (EMNLP-IJCNLP)*. Association for Computational Linguistics, 2019.

[56] J. Deng, W. Dong, R. Socher, L. Li, K. Li, and L. Fei-Fei, “ImageNet: A large-scale hierarchical image database,” in *2009 IEEE Conference on Computer Vision and Pattern Recognition*. IEEE, jun 2009.

[57] S. Fricke, “Semantic Scholar,” *Journal of the Medical Library Association: JMLA*, vol. 106, no. PMC5764585, pp. 145–147, Jan. 2018. [Online]. Available: <https://www.ncbi.nlm.nih.gov/pmc/articles/PMC5764585/>

[58] A. E. W. Johnson, T. J. Pollard, L. Shen, L. H. Lehman, M. Feng, M. Ghassemi, B. Moody, P. Szolovits, L. Anthony Celi, and R. G. Mark, “MIMIC-III, a freely accessible critical care database,” *Scientific Data*, vol. 3, no. 1, p. 160035, 2016. [Online]. Available: <https://doi.org/10.1038/sdata.2016.35>

[59] Y. Gu, R. Tinn, H. Cheng, M. Lucas, N. Usuyama, X. Liu, T. Naumann, J. Gao, and H. Poon, “Domain-Specific Language Model Pretraining for Biomedical Natural Language Processing,” *arXiv:2007.15779 [cs.CL]*, Jul. 2020.

[60] E. Alsentzer, J. Murphy, W. Boag, W.-H. Weng, D. Jindi, T. Naumann, and M. McDermott, “Publicly Available Clinical BERT Embeddings,” in *Proceedings of the 2nd Clinical Natural Language Processing Workshop*. Minneapolis, Minnesota, USA: Association for Computational Linguistics, Jun. 2019, pp. 72–78. [Online]. Available: <https://aclanthology.org/W19-1909>

[61] Y. Peng, S. Yan, and Z. Lu, “Transfer Learning in Biomedical Natural Language Processing: An Evaluation of BERT and ELMo on Ten Benchmarking Datasets,” in *Proceedings of the 18th BioNLP Workshop and Shared Task*. Association for Computational Linguistics, 2019.

[62] A. E. W. Johnson, T. J. Pollard, S. J. Berkowitz, N. R. Greenbaum, M. P. Lungren, C. ying Deng, R. G. Mark, and S. Horng, “MIMIC-CXR, a de-identified publicly available database of chest radiographs with free-text reports,” *Scientific Data*, vol. 6, no. 1, dec 2019.

[63] A. E. W. Johnson, T. J. Pollard, N. R. Greenbaum, M. P. Lungren, C. ying Deng, Y. Peng, Z. Lu, R. G. Mark, S. J. Berkowitz, and S. Horng, “MIMIC-CXR-JPG, a large publicly available database of labeled chest radiographs,” *arXiv:1901.07042 [cs.CV]*, Jan. 2019.

[64] D. Demner-Fushman, M. D. Kohli, M. B. Rosenman, S. E. Shooshan, L. Rodriguez, S. Antani, G. R. Thoma, and C. J. McDonald, “Preparing a collection of radiology examinations for distribution and retrieval,” *Journal of the American Medical Informatics Association*, vol. 23, no. 2, pp. 304–310, jul 2015.

[65] K. Papineni, S. Roukos, T. Ward, and W. Zhu, “Bleu: a Method for Automatic Evaluation of Machine Translation,” in *Proceedings of the 40th Annual Meeting of the Association for Computational Linguistics*. Philadelphia, Pennsylvania, USA: Association for Computational Linguistics, Jul. 2002, pp. 311–318. [Online]. Available: <https://www.aclweb.org/anthology/P02-1040>

[66] S. Banerjee and A. Lavie, “METEOR: An Automatic Metric for MT Evaluation with Improved Correlation with Human Judgments,” in *Proceedings of the ACL Workshop on Intrinsic and Extrinsic Evaluation Measures for Machine Translation and/or Summarization*. Ann Arbor, Michigan: Association for Computational Linguistics, Jun. 2005, pp. 65–72. [Online]. Available: <https://aclanthology.org/W05-0909>

[67] C. Lin and F. J. Och, “Automatic Evaluation of Machine Translation Quality Using Longest Common Subsequence and Skip-Bigram Statistics,” in *Proceedings of the 42nd Annual Meeting of the Association for Computational Linguistics (ACL-04)*. Barcelona, Spain, Jul. 2004, pp. 605–612. [Online]. Available: <https://aclanthology.org/P04-1077>

[68] R. Vedantam, C. Lawrence Zitnick, and D. Parikh, “CIDEr: Consensus-Based Image Description Evaluation,” in *Proceedings of the IEEE Conference on Computer Vision and Pattern Recognition (CVPR)*, June 2015.

[69] A. Smit, S. Jain, P. Rajpurkar, A. Pareek, A. Ng, and M. Lungren, “Combining Automatic Labelers and Expert Annotations for Accurate Radiology Report Labeling Using BERT,” in *Proceedings of the 2020 Conference on Empirical Methods in Natural Language Processing (EMNLP)*. Association for Computational Linguistics, Nov. 2020, pp. 1500–1519.

[70] M. Sorower, “A literature survey on algorithms for multi-label learning,” *Oregon State University, Corvallis*, vol. 18, pp. 1–25, 2010.

[71] R. J. Williams and D. Zipser, “A Learning Algorithm for Continually Running Fully Recurrent Neural Networks,” *Neural Computation*, vol. 1, no. 2, pp. 270–280, jun 1989.

[72] B. Simsek, F. Ged, A. Jacot, F. Spadaro, C. Hongler, W. Gerstner, and J. Brea, “Geometry of the Loss Landscape in Overparameterized Neural Networks: Symmetries and Invariances,” in *Proceedings of the 38th International Conference on Machine Learning*, ser. Proceedings of Machine Learning Research, M. Meila and T. Zhang, Eds., vol. 139. PMLR, 18–24 Jul 2021, pp. 9722–9732. [Online]. Available: <https://proceedings.mlr.press/v139/simsek21a.html>

[73] I. Loshchilov and F. Hutter, “Decoupled Weight Decay Regularization,” in *International Conference on Learning Representations*, 2019. [Online]. Available: <https://openreview.net/forum?id=Bkg6RiCqY7>

[74] B. Efron, “Bootstrap Methods: Another Look at the Jackknife,” *The Annals of Statistics*, vol. 7, no. 1, jan 1979.

[75] J. Libovický, J. Helcl, and D. Mareček, “Input Combination Strategies for Multi-Source Transformer Decoder,” in *Proceedings of the Third Conference on Machine Translation (WMT)*, vol. 1. Association for Computational Linguistics, 2018, pp. 253–260.

[76] T. Xiao, M. Singh, E. Mintun, T. Darrell, P. Dollár, and R. Girshick, “Early Convolutions Help Transformers See Better,” *arXiv:2106.14881 [cs.CV]*, Jun. 2021.